# Experimental mechanical and chemical compaction of carbonate sand

D. Croizé, K. Bjorlykke, J. Jahren, F. Renard

# Experimental mechanical and chemical compaction of carbonate sand

Delphine Croizé,[1,2] Knut Bjørlykke,[1] Jens Jahren,[1] and François Renard[2,3]

Received 12 May 2010; revised 11 August 2010; accepted 20 August 2010; published 25 November 2010.

[1] Uniaxial compression tests were conducted on bioclastic sand and crushed calcite crystals. Mechanical and chemical processes were investigated to better quantify petrophysical properties of carbonates and their evolution with burial or during fault zone processes. The grain size was in the range 63–500 $\mu$m, and the samples were saturated with water in equilibrium with carbonate, glycol, decane, or air. During loading, effective stress was increased to 32 MPa. Mechanical compaction processes (i.e., grain rearrangement, crushing) could be separated from chemical processes (i.e., pressure solution, subcritical crack growth). *P* and *S* waves monitored during the tests showed low velocity in samples saturated with reactive fluids. This suggested that chemical reactions at grain contacts reduced the grain framework stiffness. Creep tests were also carried out on bioclastic sand at effective stress of 10, 20, and 30 MPa. No creep was observed in samples saturated with nonreactive fluids. For all the samples saturated with reactive fluids, strain as a function of time was described by a power law of time with a single exponent close to 0.23. Parameters controlling creep rate were, in order of importance, grain size, effective stress, and water saturation. Microstructural observations showed that compaction of bioclastic carbonate sand occurred both mechanically and chemically. Crack propagation probably contributed to mechanical compaction and enhanced chemical compaction during creep. Experimental compaction showed that compaction of carbonates should be modeled as a function of both mechanical and chemical processes, also at relatively shallow depth and low temperature.

**Citation:** Croizé, D., K. Bjørlykke, J. Jahren, and F. Renard (2010), Experimental mechanical and chemical compaction of carbonate sand, *J. Geophys. Res.*, *115*, B11204, doi:10.1029/2010JB007697.

## 1. Introduction

[2] Compaction of sediments, i.e., porosity loss and density increase, induces changes in petrophysical properties of rocks. These petrophysical properties are crucial to for instance, model the stability of slopes, or for the determination of the elastic properties of the medium to image reservoirs using seismic waves or electromagnetic signals. Processes leading to porosity loss in sediments may be divided into mechanical compaction which is a function of stress, and chemical compaction which is controlled by the thermodynamics and kinetics of fluid-rock interactions [*Bjørlykke*, 2003]. Pressure solution and subcritical crack growth (stress corrosion) are two irreversible deformation processes responsible of sediments compaction that are occurring in presence of reactive fluids [*Weyl*, 1959; *Atkinson*, 1982]. Even though these deformation mechanisms are driven by stress, they are here considered as chemical compaction processes since their rate is controlled by chemical reactions such as fluid-rock reactions or diffusion in a fluid phase. In carbonate sediments, unlike siliceous sediments, mechanical and chemical processes occur simultaneously from the surface, affecting each other [*Athy*, 1930; *Weller*, 1959; *Fruth et al.*, 1966; *Schmoker and Halley*, 1982; *Bassinot et al.*, 1993; *Ehrenberg*, 2006]. In carbonate sediments the interaction between the different mechanical and chemical compaction processes, and the effect of the various initial conditions and their relation to diagenetic changes make porosity prediction difficult.

[3] The primary porosity of carbonates at the surface ranges from 50 to 70% [*Hamilton*, 1976; *Schmoker and Halley*, 1982; *Fabricius*, 2003], grain rearrangement may therefore be an important process of compaction during the first hundreds of meters. Then, when sediments reach a locked state, grain crushing becomes the main mechanism of mechanical compaction [*Chuhan et al.*, 2002; *Karner et al.*, 2005]. Stress-independent dissolution of thermodynamically unstable minerals, e.g., aragonite or magnesian calcite,

[1]Department of Geosciences, University of Oslo, Blindern, Oslo, Norway.
[2]LGCA, Université Joseph Fourier-Grenoble I, CNRS-Observatoire de Grenoble, Grenoble, France.
[3]Physics of Geological Processes, University of Oslo, Blindern, Oslo, Norway.


0148-0227/10/2010JB007697

**Table 1.** Experimental Conditions for the Uniaxial Compaction Tests[a]

| Mineralogy | d[b] | Pore Fluid | $\Phi_i$[c] | Exp[d] |
|---|---|---|---|---|
| | | *Room Temperature* | | |
| Carbonate sand | 250–500 | 5% $NH_4Cl$ solution saturated with respect to carbonate | 52.1 | T23 |
| | | Water saturated with respect to carbonate | 50.8 | T30 |
| | | Dry | 61.0 | T10 |
| | 125–250 | 5% $NH_4Cl$ solution saturated with respect to carbonate | 60.7, 61.7, 61.0, 55.7 | T15, T16, T17, T35 |
| | | Water saturated with respect to carbonate | 61.8, 55.7 | T18, T31 |
| | | Water saturated with respect to carbonate | 61.8, 55.7 | T18, T31 |
| | | N decane | 53.9, 54.9 | T20, T22 |
| | | Dry | 61.2, 53.0 | T19, T21 |
| | 63–125 | 5% $NH_4Cl$ solution saturated with respect to carbonate | 59.6 | T34 |
| | | Water saturated with respect to carbonate | 59.1 | T29 |
| | | 50% water saturated | 59.49 | T33 |
| | | with respect to carbonate, 50% Glycol | 59.49 | T33 |
| | | 97% Glycol | 51.1 | T36 |
| | | Dry | 58.9, 59.33 | T28, T32 |
| Calcite | 250–500 | Water saturated with respect to calcite | 43.0, 44.9 | T24, T26 |
| | | Dry | 44.5 | T25 |
| | 125–250 | Dry | 47.6 | T27 |
| | | *50°C* | | |
| Carbonate sand | 250–500 | 5% $NH_4Cl$ solution saturated with respect to carbonate | 61.7, 61.6 | T7, T8 |
| | | N decane | 53.1 | T12 |
| | | Dry | 60.6 | T11 |
| Calcite | 100–500 | 5% $NH_4Cl$ solution saturated | 44.6 | T13 |
| | | with respect to carbonate | 44.6 | T13 |

[a]The uniaxial stress was increased from 0 to 32 MPa.
[b]Grain size in $\mu$m.
[c]Initial porosity in percent.
[d]Experiment identification number.

followed by precipitation of calcite and dolomite may also occur at shallow depth [*Athy*, 1930; *Weller*, 1959]. When carbonate sediments contain unstable minerals early diagenesis may produce a strong framework mechanically stable preventing further mechanical compaction [*McLimans and Videtich*, 1989; *Kopaska-Merkel et al.*, 1994; *Croizé et al.*, 2010a]. In such situation porosity loss will proceed by pressure solution creep [*Weyl*, 1959] or a combination of subcritical crack growth and pressure solution [*Atkinson*, 1982].

[4] Compaction curves, i.e., porosity or density versus depth curves, are used as an input for basin modeling and prediction of reservoir properties [*Sclater and Christie*, 1980; *Audet and Fowler*, 1992; *Goldhammer*, 1997; *Giles*, 1997]. In these studies, porosity loss is often described as an exponential function of stress. However, chemical processes during burial of carbonate sediments make prediction of the relation between porosity and depth more challenging. Experimental compaction studies provide quantitative data by linking various initial conditions to physical properties as a function of stress and fluid content and may simulate both mechanical and chemical compaction.

[5] To image reservoirs, inversion of seismic data needs to be done having a rather good understanding of the relation between elastic wave propagation velocity and rock properties [*Christensen and Szymanski*, 1991]. However, seismic wave propagation is strongly affected by porosity [*Rafavich et al.*, 1984] and the type of pore in presence [*Anselmetti and Eberli*, 1993]. Seismic properties of rocks also depend on microstructures [*Wang*, 1997], fractures and cracks especially affecting *S* wave propagation [*Dürrast and Siegesmund*, 1999; *Couvreur et al.*, 2001], pore fluids [*Assefa et al.*, 2003], and grain size, shape and sorting [*Eberli et al.*, 2003]. The additional difficulty inherent to carbonate rocks is the influence of fluid-rock interactions on *P* and *S* waves measurements [*Vanorio et al.*, 2008].

[6] The present study considers two type of carbonates. While calcite has been used in a number of pressure solution studies, bioclastic carbonates sand have been less studied but may be more representative of natural sediments. The purpose of the present study is to quantify both mechanical and chemical compaction of these two materials. To this end, bioclastic carbonates and crushed calcite crystals were uniaxially compacted up to 32 MPa effective stress under drained conditions. In addition creep tests were carried out at constant vertical stresses of 10, 20, and 30 MPa. The influence of pore fluid chemistry, grain size, mineralogy, applied uniaxial stress and temperature was investigated. Ultrasonic *P* and *S* wave velocities were recorded during experiments. This study made possible to separate the respective influence of mechanical and chemical mechanisms in carbonate compaction, and to link them to the evolution of specific petrophysical properties, as well as with *P* and *S* waves ultrasonic velocity.

## 2. Materials and Methods

### 2.1. Samples and Analyses

[7] Two different materials were used. First, Holocene shell fragments from beaches near Tromsø, northern Norway, are primarily composed of magnesian calcite, i.e., high-magnesium calcite, with minor siliceous impurities. Secondly, calcite crystals (Wards international) consisting of more than 99% calcite were used. The samples were crushed, sieved, and separated into three grain size fractions. The grain size fractions used were very fine, 0.063 to 0.125 mm, fine, 0.125 to 0.250 mm, and medium, 0.250 to 0.500 mm. The main difference between the two types of

**Table 2.** Experimental Conditions for the Creep Compaction Tests[a]

| $\sigma_1$[b] | d[c] | Pore Fluid | $\Phi_0$[d] | Exp[e] |
|---|---|---|---|---|
| | | *Room Temperature* | | |
| 30 | 250–500 | 5% $NH_4Cl$ solution saturated with respect to carbonate | 27.87 | T23 |
| | | Anisole | 48.23 | T6 |
| | | Dry | 43.57 | T10 |
| | 125–250 | 5% $NH_4Cl$ solution saturated with respect to carbonate | 29.39 | T35 |
| | 63–125 | 5% $NH_4Cl$ solution saturated with respect to carbonate | 33.26 | T34 |
| | | 50% water saturated with respect to carbonate, 50% Glycol | 32.87 | T33 |
| | | 97% Glycol | 29.22 | T36 |
| | | Dry | 39.46 | T32 |
| 10 | 63–125 | 5% $NH_4Cl$ solution saturated with respect to carbonate | 35.22 | T37 |
| 20 | 63–125 | 5% $NH_4Cl$ solution saturated with respect to carbonate | 31.15 | T38 |
| | | *50°C* | | |
| 30 | 250–500 | 5% $NH_4Cl$ solution saturated with respect to carbonate | 37.49, 36.37 | T7, T8 |
| | | N decane | 36.17 | T12 |
| | | Dry | 43.41 | T11 |
| | | *80°C* | | |
| 30 | 250–500 | 5% $NH_4Cl$ solution saturated with respect to carbonate | 26.22 | T39 |

[a]All the experiments were conducted at constant stress on bioclastic carbonate sands.
[b]Constant applied stress in MPa.
[c]G grain size in $\mu$m.
[d]Porosity at the beginning of the creep test in percent.
[e]Experiment identification number.

samples is that the bioclastic sand contains mostly microporous shells of moluscs, while the calcite samples are constituted of rhomboedra with no microporosity. Magnesian calcite being more reactive than calcite, chemical compaction is therefore easier to observe in bioclastic carbonate sand under laboratory conditions. The samples were saturated with various fluids having different reactivity with respect to calcite. Nonreactive fluids used were air and N-decane. Reactive fluids were water saturated with carbonate, water with 5% $NH_4Cl$ saturated with carbonate, and mixtures of water and glycol (see Tables 1 and 2). Pore water composition was analyzed before and after some experiments. The cations were analyzed using an atomic absorption spectrometer from Varian Inc.

### 2.2. Uniaxial Compression Tests

[8] Drained uniaxial compression tests were carried out to study the compaction of carbonate sand. The samples were cylindrical with a radius of 2.5 cm and a height up to 3.1 cm. Two odometers were used (Figure 1), one of them was equipped with *P* and *S* waves receivers and senders, which were glued onto the top and bottom filters.

[9] The volume of sand, $V_s$, poured into the odometer cell was determined from the known mass of the sample and the assumed grain density, $\rho$ = 2.7 g cm$^{-3}$. The initial height allowed to determine the initial volume of the samples, $V_{ti}$. Values of initial porosities, $\Phi_i = (V_{ti} - V_s)/V_{ti}$, are given in Table 1.

[10] The load was controlled by a computer so that the vertical stress, $\sigma_1$, could be applied automatically at a given loading rate. A pore pressure sensor fixed at the bottom outlet of the odometer allowed to control the pore pressure, $P_p$, in the samples. This enabled the determination of the applied effective stress $\sigma_1' = \sigma_1 - P_p$. The pore pressure was always equal to atmospheric pressure, i.e., drained conditions. For mechanical compaction tests, the vertical stress was increased from 0 to 32 MPa at a rate of 2 MPa h$^{-1}$.

[11] In addition, creep tests were carried out at constant vertical stresses of 10, 20 or 30 MPa for about one month. All creep tests were preceded by a mechanical compaction phase where the applied stress was increased to 2 MPa higher than the creep stress. This overconsolidation made the samples mechanically stable. Therefore time-dependent deformation observed during creep was mostly due to chemical effects.

[12] Since the samples were confined into a cylindrical steel cell no lateral strain was allowed, therefore the vertical strain, $\epsilon_1$, was equivalent to the volumetric strain, $\epsilon_v$. Strain values were obtained from the vertical displacement values, $Def_1$ and $Def_2$, measured by two high-resolution displacement sensors (LVDT). Strain values were calculated as follows: $\epsilon_1 = (((Def_1 + Def_2)/2)/(h_i)) \times 100$, where $h_i$ was the initial sample's height. For all themeasured values, $\sigma_1$, $Def_1$, $Def_2$ and $P_p$, one data point per minute was recorded.

[13] Intragranular porosity, $\Phi_g$, was determined from available thin sections of the compacted samples, the mean value was found to be $\Phi_g$ = 0.27.

[14] The reproducibility of the stress-strain curves obtained was controlled for few experiments. 0.1% difference in initial porosity for tests T7 and T8 lead to 1% difference in final strain at 32 MPa stress. The 3% difference in final strain obtained for T15 and T16 may be related to the 1% difference in initial porosity. From these observations it was concluded that the results obtained were reproducible and representative of the compaction behavior of the material used.

### 2.3. Ultrasonic Velocity Measurements

[15] Compressional and shear wave velocities were measured throughout the tests at regular time intervals using the

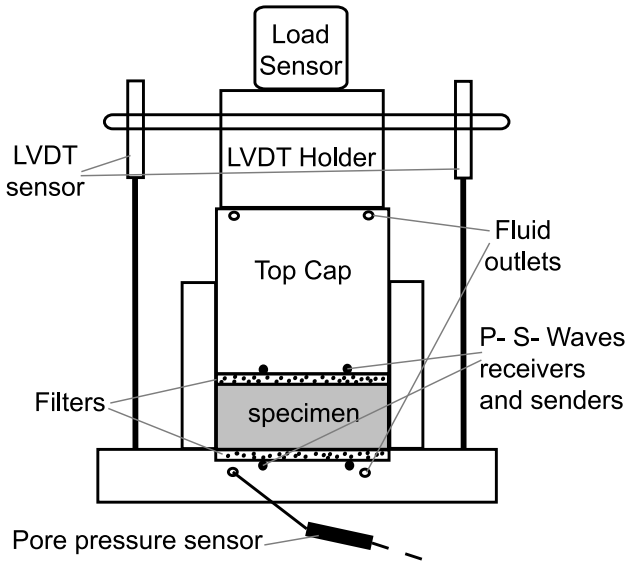


**Figure 1.** Schematic view of an odometer cell. The top cap is made of titanium grade 5; the rest of the cell is made of stainless steel.

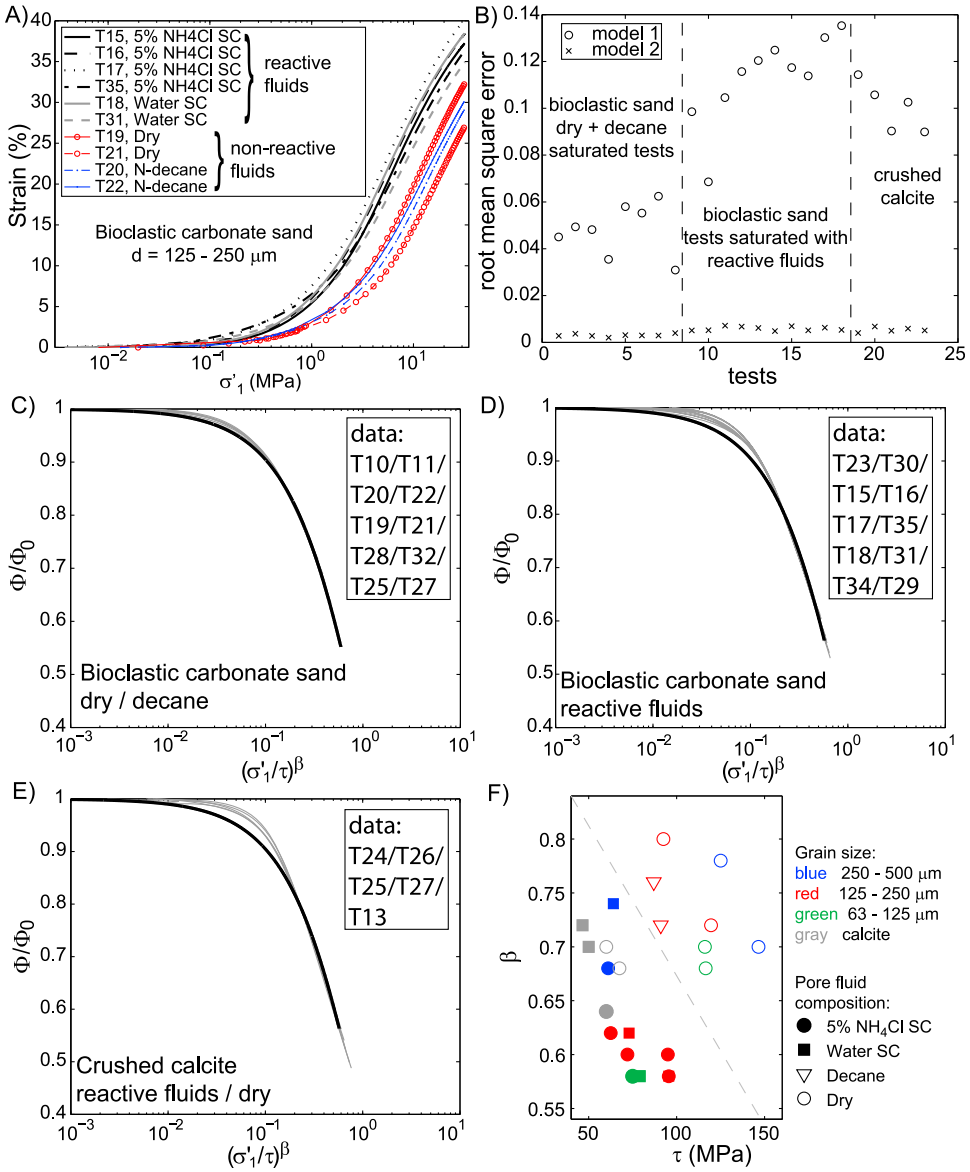


**Figure 2.** (a) Example of stress-strain relationship obtained during mechanical compaction (SC, saturated with respect to carbonate). (b) Comparison of the root-mean-square errors obtained when fitting equations (1) (model 1) and (2) (model 2) to the present experimental data. Data (gray lines) collapsed using the exponential stretched model (black line) for (c) bioclastic sand saturated with nonreactive fluids, (d) bioclastic sand saturated with reactive fluids, and (e) crushed calcite samples. (f) The $\tau$ and $\beta$ fitting parameters were used to collapsed the data onto a single curve.

pulse transmission technique [*Birch*, 1960]. *P* and *S* wave piezoelectric transducers were mounted inside the base and filters of the odometer cell to measure *P* and *S* wave velocities along the plug axis. Resonant frequency of the crystals was 500 kHz. Compressional and shear wave velocities were measured in the range 1000–2500 and 500–1250 m $s^{-1}$, respectively. Although the resonant frequency of the glued crystals may deviate somewhat from the one of the pure crystal, the wavelength of the ultrasonic pulse is assumed to range from 1 to 5 mm, which is less than the plugs radius. This arrangement is most likely sufficient to avoid diffraction phenomena and unwanted shape mode. The signals were recorded on a computer, and first arrival times were picked manually. Correction for equipment was applied to the *P* and *S* wave velocities. First arrival times, $t_0$, were measured when no sample was present in the odometer. This zero time was then subtracted from the picked traveltime, $t_{p/s}$, measured with a plug present. The plug's compressional or shear wave velocity was then calculated as follows: $V_{p/s} = h_s/(t_{p/s} - t_0)$, where $h_s$ is the height of the sample.

### 2.4. Microstructure Observation

[16] After completion of the compaction tests some of the samples were impregnated with epoxy to make thin sections of the compacted material. The central part of the sample

**Table 3.** Results of Mechanical Compaction[a]

| Exp[b] | $\Phi_0$[c] | $\Phi_5$ | $\Phi_{10}$ | $\Phi_{32}$ | $\epsilon_5$ | $\epsilon_{10}$ | $\epsilon_{32}$ | $V_{p5}$ | $V_{p10}$ | $V_{p32}$ | $V_{s5}$ | $V_{s10}$ | $V_{s32}$ |
|---|---|---|---|---|---|---|---|---|---|---|---|---|---|
| T23 | 52.1 | 43.91 | 38.45 | 28.12 | 14.53 | 22.02 | 32.85 | 1306 | 1670 | 2400 | 713 | 924 | 1249 |
| T30 | 50.8 | 44.3 | 39.09 | 28.63 | 11.53 | 19 | 30.52 | 1337 | 1694 | 2402 | 699 | 898 | 1251 |
| T10 | 61 | 55.8 | 52.14 | 43.58 | 11.55 | 18.22 | 30.29 | | | | | | |
| T15 | 60.7 | 51.47 | 46.13 | 37.05 | 18.96 | 27 | 37.24 | 1329 | 1680 | 2439 | 670 | 826 | 1191 |
| T16 | 61.7 | 51.82 | 46.47 | 37.2 | 20.28 | 28.15 | 38.42 | 1267 | 1598 | 2356 | 680 | 829 | 1179 |
| T17 | 61 | 49.93 | 44.21 | 34.85 | 21.97 | 29.89 | 39.67 | 1282 | 1620 | 2309 | 662 | 824 | 1140 |
| T35 | 55.5 | 45.34 | 39.79 | 29.4 | 18.4 | 25.82 | 36.37 | 1241 | 1560 | 2233 | 668 | 840 | 1174 |
| T18 | 61.8 | 51.83 | 46.48 | 37.39 | 20.61 | 28.45 | 38.5 | 1235 | 1596 | 2329 | 682 | 834 | 1180 |
| T31 | 55.7 | 46.39 | 41.14 | 31.4 | 17.26 | 24.54 | 34.92 | 1232 | 1555 | 2250 | 674 | 836 | 1187 |
| T20 | 53.9 | 48.48 | 44.35 | 34.29 | 10.39 | 16.93 | 29.23 | 1161 | 1424 | 2020 | 603 | 759 | 1068 |
| T22 | 54.9 | 48.79 | 44.54 | 34.71 | 11.66 | 18.33 | 30.23 | 1076 | 1359 | 1976 | 593 | 749 | 1063 |
| T19 | 61.2 | 55.69 | 51.58 | 42.25 | 12.39 | 19.73 | 32.35 | 1229 | 1531 | 2126 | 650 | 806 | 1108 |
| T21 | 53 | 48.38 | 44.75 | 34.97 | 8.8 | 14.67 | 27.09 | 1208 | 1506 | 2125 | 655 | 809 | 1145 |
| T34 | 59.5 | 48.48 | 43.09 | 33.27 | 21.38 | 28.74 | 38.9 | 1178 | 1484 | 2194 | 646 | 799 | 1142 |
| T29 | 59 | 48.29 | 42.95 | 33.49 | 20.86 | 28.23 | 38.17 | 1121 | 1432 | 2067 | 613 | 773 | 1085 |
| T33 | 59.4 | 47.65 | 42.27 | 32.88 | 22.56 | 29.69 | 39.24 | 1167 | 1488 | 2188 | 632 | 789 | 1128 |
| T36 | 51.1 | 39.24 | 35.87 | 29.21 | 19.41 | 23.55 | 30.36 | 1080 | 1396 | 2065 | 590 | 748 | 1101 |
| T28 | 58.8 | 52.93 | 48.98 | 39.74 | 12.51 | 19.2 | 31.27 | 1113 | 1382 | 1958 | 596 | 747 | 1046 |
| T32 | 59.2 | 52.86 | 48.83 | 39.61 | 13.64 | 20.37 | 32.24 | 1094 | 1364 | 1938 | 606 | 760 | 1062 |
| T24 | 43 | 35.5 | 30.21 | 20.97 | 11.52 | 18.12 | 27.34 | 1545 | 1935 | 2659 | 835 | 1026 | 1403 |
| T26 | 44.9 | 37.13 | 31.91 | 22.36 | 12.26 | 18.9 | 28.55 | 1573 | 1936 | 2621 | 809 | 988 | 1359 |
| T25 | 44.5 | 37.7 | 33.01 | 24.03 | 10.78 | 16.93 | 26.41 | 1579 | 1937 | 2609 | 900 | 1064 | 1419 |
| T27 | 47.5 | 40.47 | 35.77 | 26.71 | 11.79 | 18.14 | 27.88 | 1498 | 1861 | 2530 | 834 | 1015 | 1377 |
| T7 | 61.5 | 51.75 | 46.45 | 37.52 | 20.4 | 28.3 | 38.6 | | | | | | |
| T8 | 60.9 | 50.9 | 45.41 | 36.4 | 20.98 | 28.93 | 39 | | | | | | |
| T12 | 54.1 | 49.63 | 45.94 | 36.16 | 8.8 | 14.91 | 27.56 | 1266 | 1566 | 2202 | | 820 | 1110 |
| T11 | 60.5 | 56.31 | 52.45 | 43.41 | 9.74 | 17 | 29.99 | 1297 | 1614 | 2209 | 692 | 870 | 1154 |
| T13 | 44.1 | 36.25 | 31.77 | 23.05 | 12.29 | 18.04 | 27.33 | | | | | | |

[a]Values of porosity ($\Phi$, in%), strain ($\epsilon$, in %) and $P$ and $S$ wave velocities ($V_p$ and $V_s$, in m s$^{-1}$) are given for vertical effective stress values of 5, 10, and 32 MPa (subscripts design the effective stress at which the value was taken).
[b]Experiment identification number.
[c]Initial porosity.

was used for thin sections, that were then imaged in a JEOL JSM 6460LV scanning electron microscope (SEM). About 30 scanning electron micrographs were taken per samples. Cracks were outlined manually and measured with the help of an image processing software (ImageJ). The median length value and the length distribution of the cracks were then graphically depicted using box plot display [*Velleman and Hoaglin*, 1981].

## 3. Results

### 3.1. Porosity Loss Under Increasing Stress

[17] The effects of pore fluid composition (Figure 2a), grain size and mineralogy on the stress-strain relationships were investigated. At effective stress of 32 MPa bioclastic carbonate sand samples were more compressible than crushed calcite samples (Table 3). Final strains, $\epsilon_{32}$, obtained in bioclastic carbonate sand ranged from 27.09 to 39.67%. For crushed calcite samples the range of final strains was narrower with $\epsilon_{32}$ between 26.41 and 28.55%.

[18] To further investigate the mechanisms leading to porosity loss, the present data were first fitted with the exponential law proposed by *Athy* [1930]. This law, often used to describe porosity loss in sedimentary basins, can be expressed as follows:

$$\Phi\left(\sigma'\right) = \Phi_0 \exp\left(F\sigma'\right), \tag{1}$$

with $\Phi$ the porosity, $\Phi_0$ the initial porosity, and $F$ a compaction factor which value depends upon the sediments compositions [*Royden and Keen*, 1980] and acts as a fitting parameter. Granular media compaction can alternatively be viewed as a progress of the grains from an initial perturbed configuration toward an equilibrium state involving a number of different relaxation phenomena [*Knight et al.*, 1995]. Therefore the present data were also fitted by a stretched exponential law, which best describes relaxation in disordered systems [*Philippe and Bideau*, 2002],

$$\frac{\Phi\left(\sigma'\right)}{\Phi_0} = \exp\left(-\left(\frac{\sigma'}{\tau}\right)^{\beta}\right), \tag{2}$$

with $\tau$ and $\beta$ two free parameters related to the relaxation phenomena involved. These two existing compaction models were fitted to the present set of data. The root-mean-square errors, i.e., measurement of the differences between values predicted by the models and the actual values, are displayed in Figure 2b. The fits of the data are about 20 times better when using the stretched exponential law.

[19] All the experimental data were collapsed onto a single stretched exponential curve using the relation described in equation (2) (Figures 2c, 2d, and 2e). The model fits well the bioclastic sand saturated with nonreactive fluids data. For bioclastic carbonate sand saturated with reactive fluids and crushed calcite the model initially deviates from the observed data, indicating that several mechanisms may be responsible for porosity loss at short timescale. However, the model fits well all the data after this initial stage. Different values of $\tau$ and $\beta$ were attributed to each experiment in order to obtain the best fit possible. Values of $\tau$ range

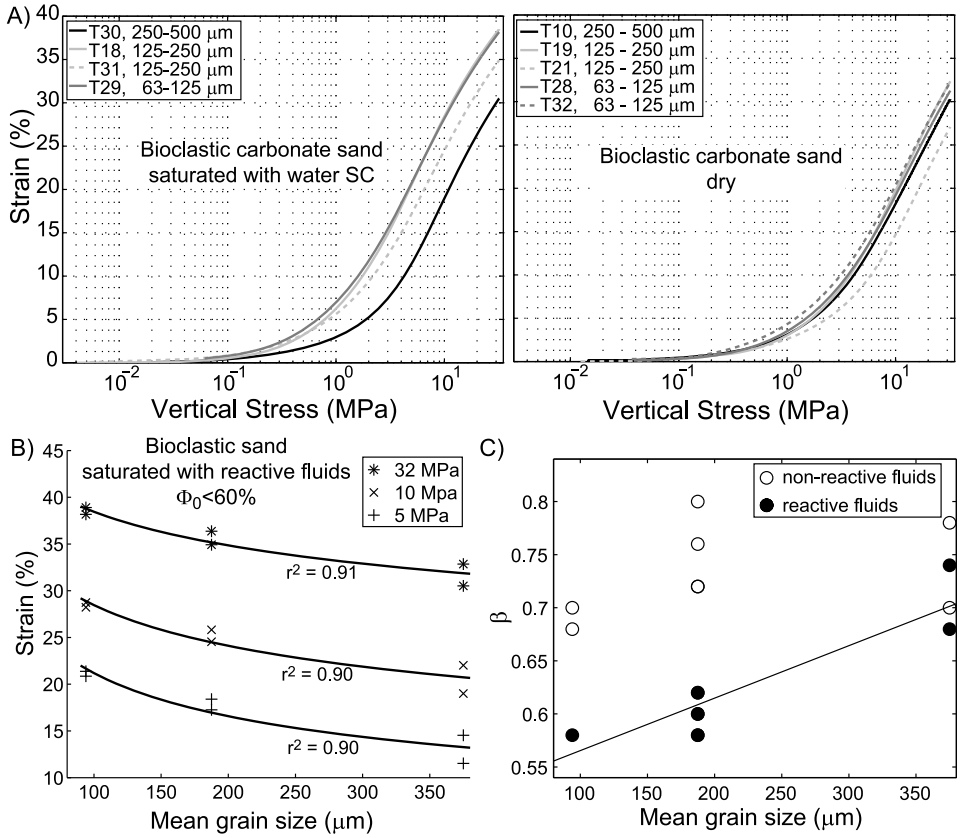


**Figure 3.** (a) Effect of the grain size on stress-strain curves for bioclastic sand either saturated with water with respect to carbonate (SC) or dry. (b) Strain-grain size relationship (equation (3)) for samples with an initial porosity lower than 60%. (c) The parameter $\beta$ (equation (2)) as a function of grain size for both samples saturated with reactive and nonreactive fluids.

between 61 and 96 MPa for experiments in which the samples were saturated with reactive fluids, between 87 and 147 MPa for samples saturated with nonreactive fluids, and between 47 and 68 MPa for calcite samples. Values of $\beta$ range between 0.58 and 0.74 for samples saturated with reactive fluids, between 0.68 and 0.80 for samples saturated with nonreactive fluids, and between 0.64 and 0.72 for calcite.

### 3.1.1. Effect of the Pore Fluid Chemistry

[20] For all the grain sizes tested, bioclastic sand was more compressible when saturated with reactive fluids (e.g., fine bioclastic carbonate sand in Figure 2a). The difference between strain, $\epsilon$, obtained in samples saturated with reactive fluids and strain in samples saturated with nonreactive fluids increased up to a vertical stress of 2 to 3 MPa. At effective stress greater than 2–3 MPa $\epsilon_{\text{reactivefluid}} - \epsilon_{\text{nonreactivefluid}}$ is rather constant. Bioclastic carbonate samples tested saturated with reactive or nonreactive fluids could be discriminated from each other using values of $\beta$ and $\tau$ obtained by fitting the data with equation (2) (grey dashed line in Figure 2f).

[21] In crushed calcite samples, unlike bioclastic carbonate sand, very little increase of compaction was observed in tests carried out with water saturated with respect to calcite compared to those conducted dry. Two percent more strain at 32 MPa occurred in T26 (water saturated with respect to calcite) compared to T25 (dry) (Table 3). No definite difference between reactive and nonreactive fluids was found for the $\beta$ and $\tau$ values (Figure 2f).

[22] Another feature was that samples saturated with glycol compacted more than samples saturated with decane (Table 3).

### 3.1.2. Effect of Grain Size

[23] In dry tests, grain size does not have a significant effect on the stress-strain relationship (Figure 3a). In bioclastic carbonate sand saturated with reactive fluids, compressibility is greater in finer samples (Figures 3a and 3b). The effect of grain size on crushed calcite samples was not tested.

[24] The initial grain rearrangement process in samples having an initial porosity greater than 60% is most likely greater than in samples starting with lower porosity. This influenced their overall compaction curve. Samples with initial porosity $\Phi_0 < 60\%$ show a good correlation between strain and grain size (Figure 3b). This correlation could be expressed as

$$\epsilon = C\frac{1}{d^n}, \tag{3}$$

with $\epsilon$ the strain in percent, $d$ the mean grain size in micrometer, and $C$ a constant. The grain size exponent, $n$, slightly decreased with increasing stress, $n$ = 0.35, 0.24, 0.14, at effective stresses of 5, 10 and 32 MPa, respectively (Figure 3b).

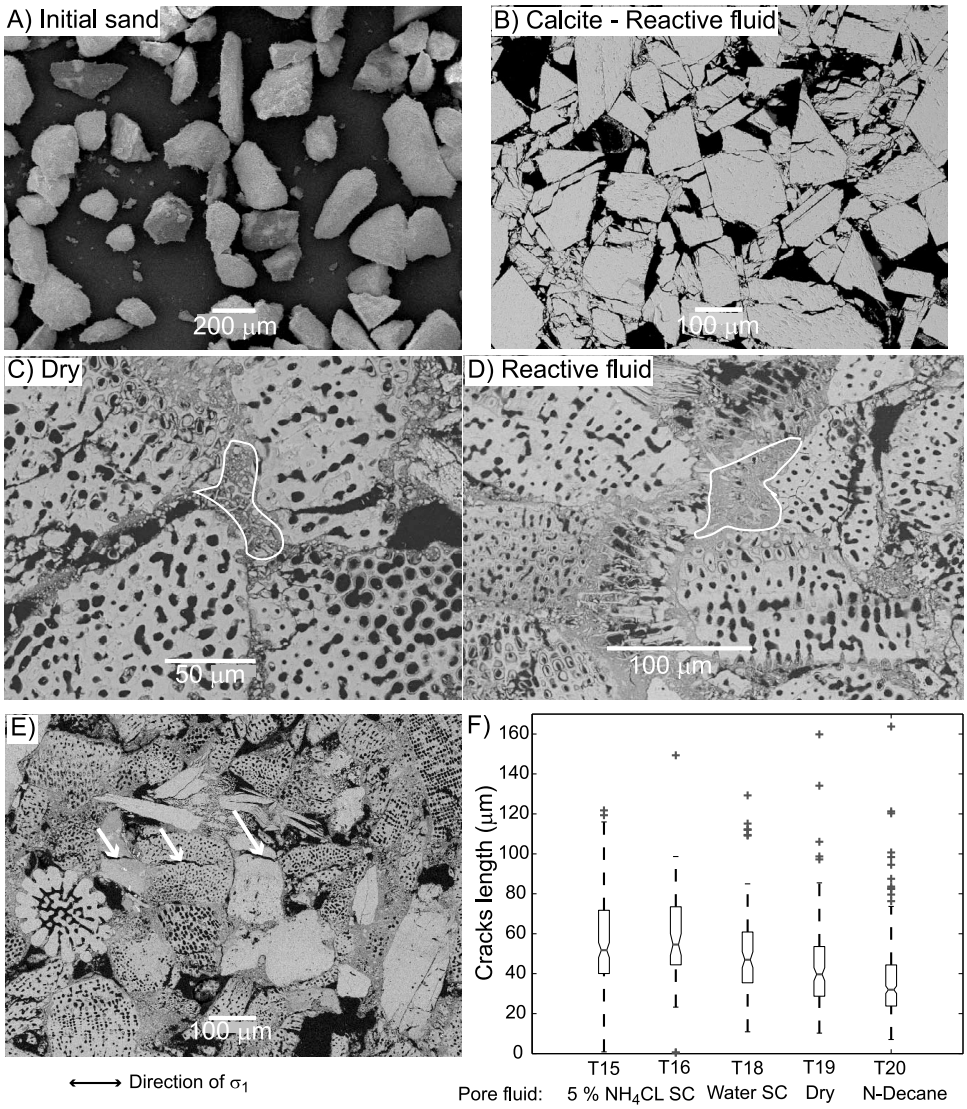


**Figure 4.** Microstructures observations. (a) Bioclastic carbonate sand of grain size 125–250 $\mu$m before experiments. Grain crushing at the grain-to-grain contacts after mechanical compaction in (b) calcite sample, (c) dry bioclastic carbonate sample, and (d) bioclastic carbonate sample saturated with reactive fluid. (e) Scanning electron micrograph of sample T18. The arrows point out the cracks parallel to the main stress axis. (f) Box plots showing the mean crack length for samples T15, T16, T18,T20, and T19, i.e., bioclastic carbonate sand samples with grain size 125–250 $\mu$m.

[25] While no correlation was found between grain size and $\beta$ (equation (2)) for samples saturated with nonreactive fluids, $\beta$ increased with grain size in samples saturated with reactive fluids (Figure 3c).

### 3.1.3. Microstructures in the Bioclastic Carbonate Sand

[26] Grain crushing or collapse of the internal grain structure on the edge of bioclastic carbonate grains was observed in thin sections (Figures 4c and 4d). The internal porosity remained unchanged in the center of each grain, while at the grain-to-grain contact internal porosity was drastically reduced. This edge deformation mechanism seems to be mainly mechanical since samples compacted dry and samples saturated with reactive fluids show about the same deformation pattern. The crushed rims appear, however, slightly thicker in samples saturated with reactive fluids (Figures 4c and 4d). In crushed calcite samples the crack density is higher compared to the bioclastic carbonate samples (Figure 4b).

[27] Thin sections also showed that crack propagation occurred during experiments (Figure 4e). Crack length correlated positively with carbonate solubility in the different fluids used (Figure 4f), which might be an indication that subcritical crack growth was active [*Anderson and Grew*, 1977].

### 3.1.4. Ultrasonic Velocity Measurements Under Increasing Stress

[28] $P$ and $S$ wave velocities increased with increasing stress and decreasing porosity, for all grain sizes and pore fluid compositions tested (Table 3). The increase of $P$ and $S$ waves with decreasing porosity was linear. $V_p$ ranged from 705 to 2440 m s$^{-1}$ and $V_s$ from 535 to 1250 m s$^{-1}$. In

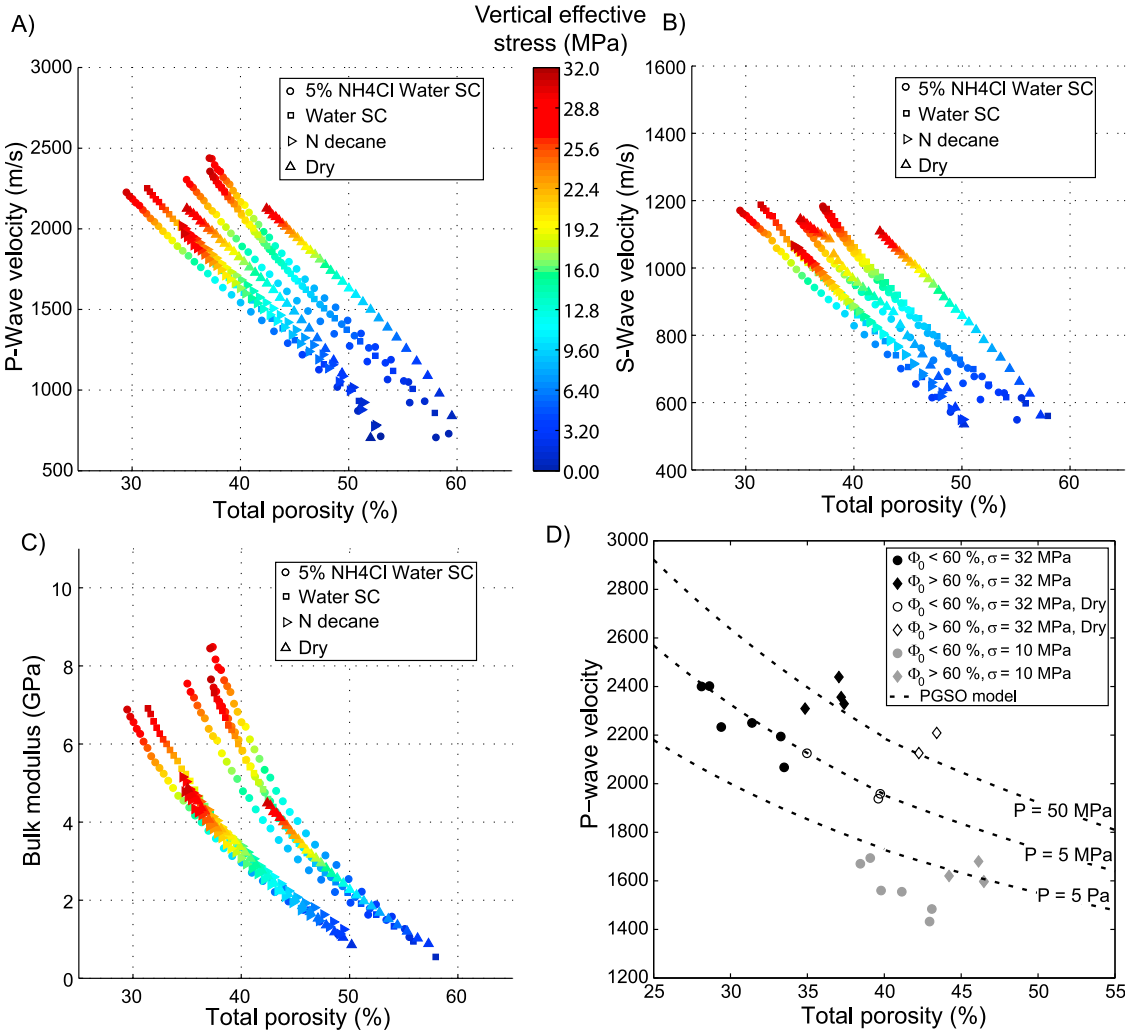


**Figure 5.** (a) *P* wave velocities, (b) *S* wave velocities, and (c) bulk moduli as a function of porosity for bioclastic carbonate sand (d = 125–250 $\mu$m) saturated with various fluids. The color represents the applied vertical effective stress. (d) *P* wave velocity for all the samples tested as a function of total porosity. Samples saturated with reactive fluids are black ($\sigma_1$ = 32 MPa) or gray ($\sigma_1$ = 10 MPa), and dry samples are open. Dashed lines correspond to results obtained with the PGSO model [*Ruiz and Dvorkin*, 2009].

Figures 5a, 5b, and 5c, $V_p$, $V_s$, and bulk moduli are displayed as a function of porosity for 10 samples. The samples can be split in two groups characterized by different initial porosities. Even though the initial sample porosities were different, the initial velocity measurements are similar indicating a strong effect of the applied vertical effective stress on the ultrasonic velocity measurements.

[29] At a given vertical effective stress, bulk moduli of samples saturated with reactive fluids are greater than bulk moduli of samples saturated with nonreactive fluids (Figure 5c). The two different initial porosity groups show the same bulk modulus-porosity relationship.

[30] To investigate further the effect of effective stress, pore fluid composition, and porosity on the propagation of ultrasonic waves in the present bioclastic carbonate sand, data were compared to a rock physics porous-grain soft-sand model (PGSO) similar to the model described by *Ruiz and Dvorkin* [2009] (Figure 5d). This model considers the samples as a pack of elastic porous grains. The effective bulk and shear moduli of the dry granular frame, $K_{dry}$ and $\mu_{dry}$, were obtained from equations (3)–(5) of *Ruiz and Dvorkin* [2009]. The Hertz-Mindlin moduli at the critical porosity, $\Phi_c$ = 0.4, were calculated using a coordination number of 5 [see *Ruiz and Dvorkin*, 2009, equation (4)]. Effective bulk and shear moduli of the porous grains, $K_g$ and $\mu_g$, were determined using the differential effective medium model [*Norris*, 1985; *Mavko et al.*, 2009]. In the present study, the inclusion were considered as spherical and the coupled system of differential equations was solved using spheres inclusion shape coefficients [*Berryman*, 1995; *Mavko et al.*, 2009]. The inclusions volumetric concentration was set equal to the internal porosity of the grain, $\Phi_g$, and were filled with water. Saturated bulk moduli, $K_{sat}$, were calculated following *Gassmann* [1951] fluid substitution theory.

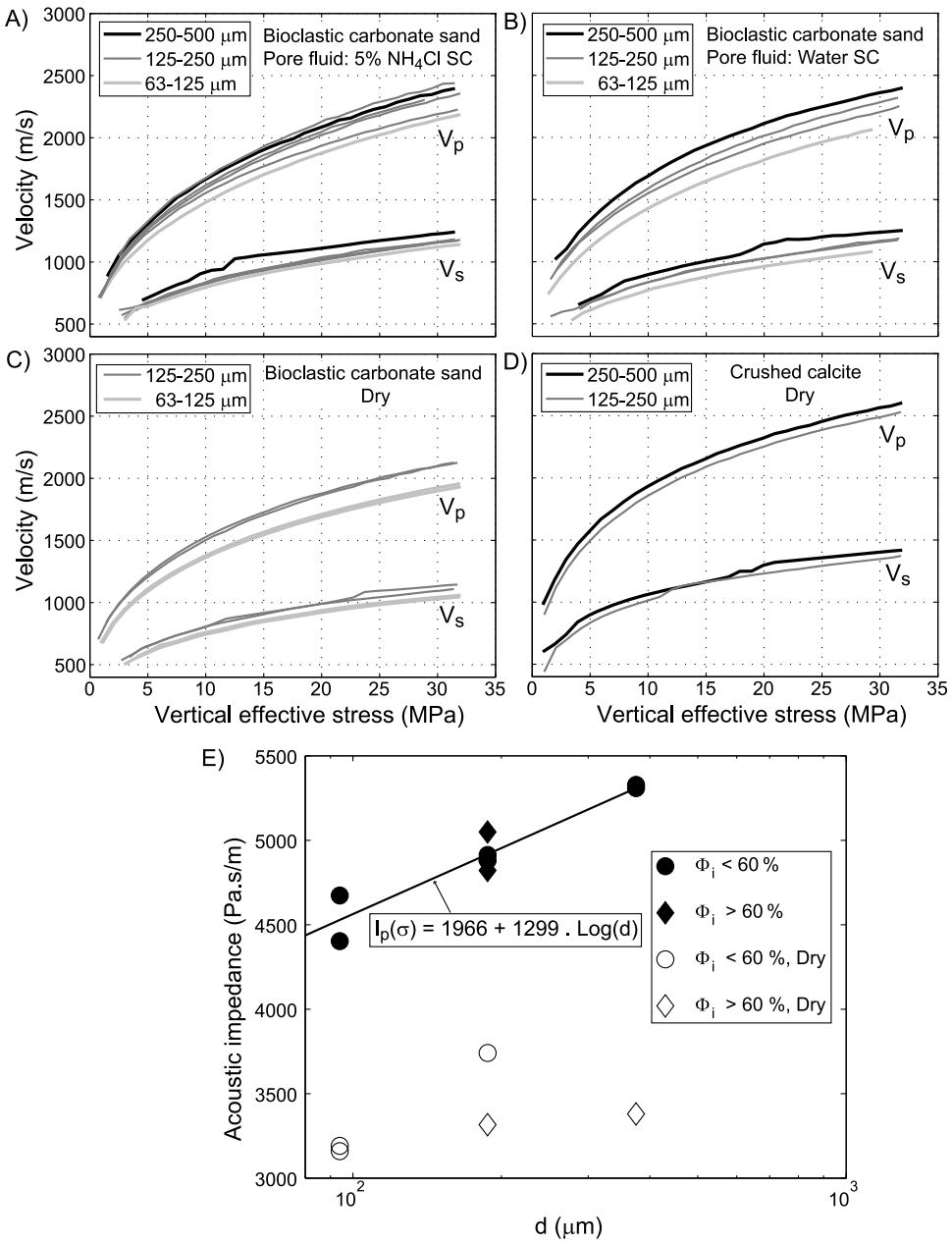


**Figure 6.** Effect of grain size on $V_p$ and $V_s$ as a function of stress for (a and b) bioclastic carbonate sand saturated with reactive fluids, (c) dry bioclastic carbonate sand, and (d) dry crushed calcite. (e) Acoustic impedance at 32 MPa vertical effective stress as a function of grain size for dry samples and samples saturated with reactive fluids.

[31] At effective stress greater than 10 MPa, it was possible to compare the present data to the PGSO model (Figure 5d). *P* wave velocities at 32 MPa effective stress were plotted against porosities for samples saturated with reactive fluids and dry samples (Figure 5d). Figure 5d separates data into two groups. The first group (tests T19, T15, T16 and T18) have initial porosities greater than 60%, while the second group (tests T20, T21, T22, T31 and T35) have porosities lower than 60% (Table 1). The PGSO model was used to fit the data varying values of differential pressures, *P*, acting on the grains from 5 Pa to 50 MPa. Samples with greater initial porosities display higher *P* wave velocities and could be fitted by a PGSO model with *P* = 50 MPa, while a *P* equal to 5 MPa fitted the samples having initial porosities lower than 60%. The dry samples had less porosity and lower *P* wave velocity but could be fitted the same way than the saturated samples having velocity lower than expected by the theory.

[32] *P* and *S* wave velocities increased with increasing grain size in both bioclastic carbonate sand and crushed calcite samples (Figures 6a, 6b, 6c, and 6d). A positive correlation exists between the *P* wave acoustic impedance, $I_p = V_p\rho$, and grain size,

$$I_p(\sigma) = A + B\log(d); \tag{4}$$

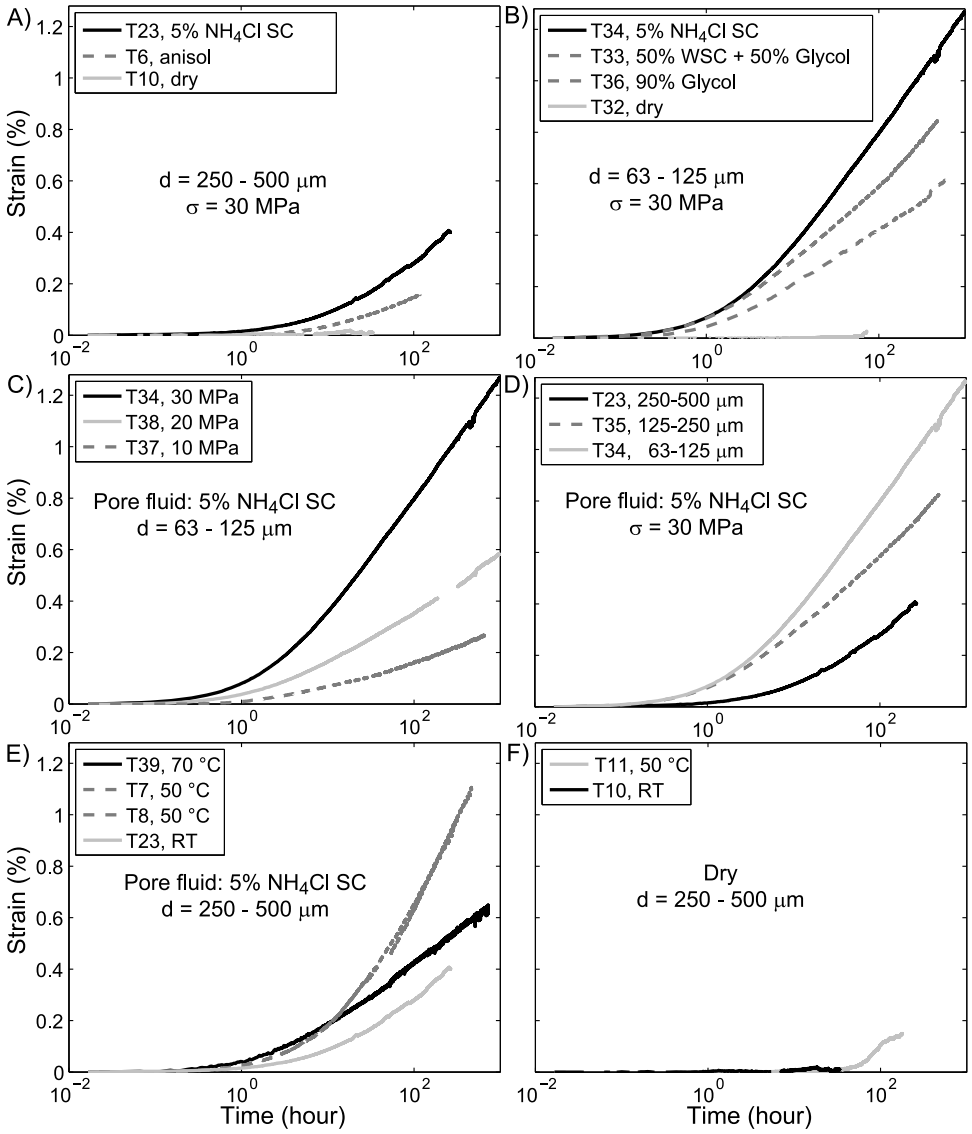


**Figure 7.** Strain versus time (logarithm scale for the time) for creep of bioclastic carbonate sand. If not specified, the tests were run at room temperature. (a and b) Effect of the pore fluid composition for two different grain sizes, (c) effect of applied vertical effective stress, (d) effect of the grain size, and (e and f) effect of the temperature.

where $I_p(\sigma)$ is the $P$ wave acoustic impedance at a given stress and $d$ is the mean grain size. Good correlation was obtained for samples saturated with reactive fluids (Figure 6e). No satisfactory relation between acoustic impedance and grain size was found for the dry samples.

## 3.2. Creep

### 3.2.1. Effect of Pore Fluid Composition, Grain Size, Temperature, and Stress

[33] No deformation was observed during creep of samples saturated with nonreactive fluids, i.e., air or decane. Significant deformation was, however, observed in samples saturated with a solution of 5% $NH_4Cl$ water in equilibrium with carbonates or in samples saturated with glycol or anisole. The amount of strain found in samples saturated with reactive fluids increased with water saturation (Figures 7a and 7b), applied stress (Figure 7c), and decreasing grain size (Figure 7d). Only a minor temperature effect was observed on samples saturated with reactive fluids (Figure 7e), and no effect was observed on the dry samples (Figure 7f), the range of temperatures used in the various experiments was small, however.

[34] Both magnesium and calcium concentration increased in the pore water during the water saturated tests (Table 5). The $[Mg^{2+}]/[Ca^{2+}]$ ratio in the pore water also increased resulting in a relative buildup of magnesium concentration in the pore water.

[35] In glycol or anisole saturated samples, the measured strain values were intermediate between dry samples and samples saturated with a solution of 5% $NH_4Cl$ water in equilibrium with carbonate (Figure 7 and Table 4). Increasing the water/glycol ratio also enhanced compaction.

**Table 4.** Creep Results[a]

| Exp | $\epsilon_{40h}$ | $\epsilon_{100h}$ | $\epsilon_{250h}$ | $\alpha$[b] | $p$[c] | $V_{p40h}$ | $V_{p100h}$ | $V_{p150h}$ | $V_{s40h}$ | $V_{s100h}$ | $V_{s150h}$ |
|---|---|---|---|---|---|---|---|---|---|---|---|
| T23 | 0.19 | 0.28 | 0.40 | 0.11 | 0.65 | 2521 | 2545 | 2575 | 1304 | 1317 | 1330 |
| T6 | 0.09 | 0.15 | | 0.05 | | | | | | | |
| T35 | 0.46 | 0.59 | 0.72 | 0.21 | 0.90 | 2347 | 2395 | 2423 | 1323 | 1244 | 1256 |
| T34 | 0.62 | 0.80 | 0.98 | 0.27 | 0.92 | 2307 | 2343 | 2395 | 1197 | 1228 | 1244 |
| T33 | 0.47 | 0.59 | 0.73 | 0.20 | 0.89 | 2301 | 2338 | 2372 | 1170 | 1197 | 1223 |
| T36 | 0.34 | 0.42 | 0.50 | 0.14 | 0.95 | 2162 | 2174 | 2222 | 1136 | 1163 | 1175 |
| T37 | 0.12 | 0.16 | 0.21 | 0.06 | 0.83 | 1693 | 1707 | 1713 | 867 | 875 | 888 |
| T38 | 0.27 | 0.35 | 0.47 | 0.12 | 0.87 | 2084 | 2109 | 2156 | 1094 | 1100 | 1116 |
| T7 | 0.43 | 0.65 | 0.91 | 0.25 | 0.75 | | | | | | |
| T8 | 0.47 | 0.68 | 0.92 | 0.25 | 0.75 | | | | | | |
| T39 | 0.31 | 0.42 | 0.52 | 0.14 | 0.87 | 2493 | 2552 | 2617 | 1276 | 1296 | 1309 |

[a]Values of strain and $P$ and $S$ wave velocity after 40, 100 and 250 h of creep.
[b] Values of the fitting parameters $\alpha$ and $p$ in equation (5) as $\alpha_j$.
[c]In equation (7).

[36] To better understand the parameters controlling creep in the present study, the entire data set was fitted with a power law of time, $t$ (Figure 8a),

$$\epsilon_j(t) = \alpha_j t^{\theta}, \tag{5}$$

with $j$ between 1 and 11, the number of creep experiments taken into consideration. In the present study the time exponent $\theta$ is close to 0.23 for all experiments. The compaction parameter, $\alpha_j$, was used as a scaling parameter to collapse all the data on the theoretical curve (black line Figure 8a) for which $\alpha = 1$. Since $\alpha$ is a time-independent factor, it is possible to quantify the respective influence of the tested parameters alone [*Renard et al.*, 2001].

[37] Grain size, $d$, vertical effective stress, $\sigma$, and water saturation, $w$, affected creep of bioclastic carbonate sand in various ways (Figure 8 and Table 4). The compaction parameter, $\alpha$, could be expressed as a function of the above mentioned parameters as follows:

$$\alpha = c_1 \exp(c_2 d + c_3 \sigma) + c_4 w + c_5, \tag{6}$$

with $c_1$, $c_2$, $c_3$, $c_4$, and $c_5$ material-dependent constants. Creep deformation was mostly affected by grain size, then by the applied vertical effective stress and to a lesser extent by the water concentration resulting in the following ranking of equation (6) parameters: $c_2 \gg c_3 \gg c_4$ (Figures 8b, 8c, and 8d).

[38] The samples compacted at 50 and 70°C both showed more creep than the sample compacted at room temperature (Figure 7e and Table 4). More deformation was observed in samples at 50°C than the one at 70°C probably related to higher initial porosities in tests T7 and T8. Tests T23 and T39 with similar starting porosity also showed a similar creep development. However, the temperature effect was rather small, with $\alpha$ increasing from 0.11 to 0.14 for $T$ increasing from 22°C to 70°C.

[39] For power law creep, with a low value of the exponent, there is for some materials a possibility that the creep does not behave as a power law, but rather like a logarithm in time. To test this hypothesis, the strain rates (with a slope of −1 in the case of logarithmic creep) rather than the strain should be fitted. This hypothesis was tested. The strain rates, $\partial\epsilon/\partial t = \dot{\epsilon}$, decreased from $1.26 \times 10^{-3}$–$1.97 \times 10^{-4}$ to $1.71 \times 10^{-4}$–$1.69 \times 10^{-6}$ min$^{-1}$.

[40] In the present study, a linear strain rate decrease in the log-log space as a function of time was observed after 200 min of creep (Figure 8e), and could be expressed as a power law:

$$\dot{\epsilon} = E t^{-p}, \tag{7}$$

with $p$ the strain rate decay exponent and $E$ a constant. The strain rate decay exponent $p$ was somewhat affected by the different parameters tested (Figure 8f), but was always significantly smaller than 1 (Table 4), indicating that the power law in time best represent the best fit.

#### 3.2.2. Ultrasonic Velocity Measurements During Creep

[41] During creep tests, $P$ and $S$ wave velocities increased linearly with strain, $V_{p/s} = a\epsilon + b$. The $V_p$ to $V_s$ ratio stayed constant during creep tests and was comprised between 1.9 and 2.0 for all the tests. The effects of pore fluid, grain size, and applied uniaxial stress on velocity is shown in Figure 9. $S$ wave velocity was not affected by the pore fluid composition, and was influenced in a similar way as $P$ wave velocity by grain size and applied stress. Samples saturated with water or with a mixture of 50% water and 50% glycol had the same $P$ wave velocity while the samples saturated with 97% glycol showed lower velocities (Figure 9a). $V_p$ increased of 8% in water saturated samples (T34, T33) from the end of the loading phase until 250 h of creep. For the same period of time, a smaller velocity increase was observed when the sample was saturated with 97% glycol, i.e., 7% increase in test T36 (Table 4).

[42] As observed during the initial mechanical phase of the tests, $P$ and $S$ wave velocities increased with increasing grain size and stress (Figures 9b and 9c). However, compaction being faster in finer grained samples, velocity also increased faster, i.e., 8.4% increase from the end of the loading phase to 250 h of creep in T34 against 6.8% in T23 (Table 4).

## 4. Discussion

### 4.1. Porosity Loss With Increasing Stress

#### 4.1.1. Effect of Carbonate Dissolution

[43] The amount of chemical compaction is given by the difference between the strain in samples saturated with reactive fluids and the lower strain in samples saturated with nonreactive fluids. Chemical compaction rate being controlled by diffusion or reaction kinetics, its observed amount is therefore related to the loading rate used (2 MPa h$^{-1}$), i.e., slower loading rate would produce greater difference

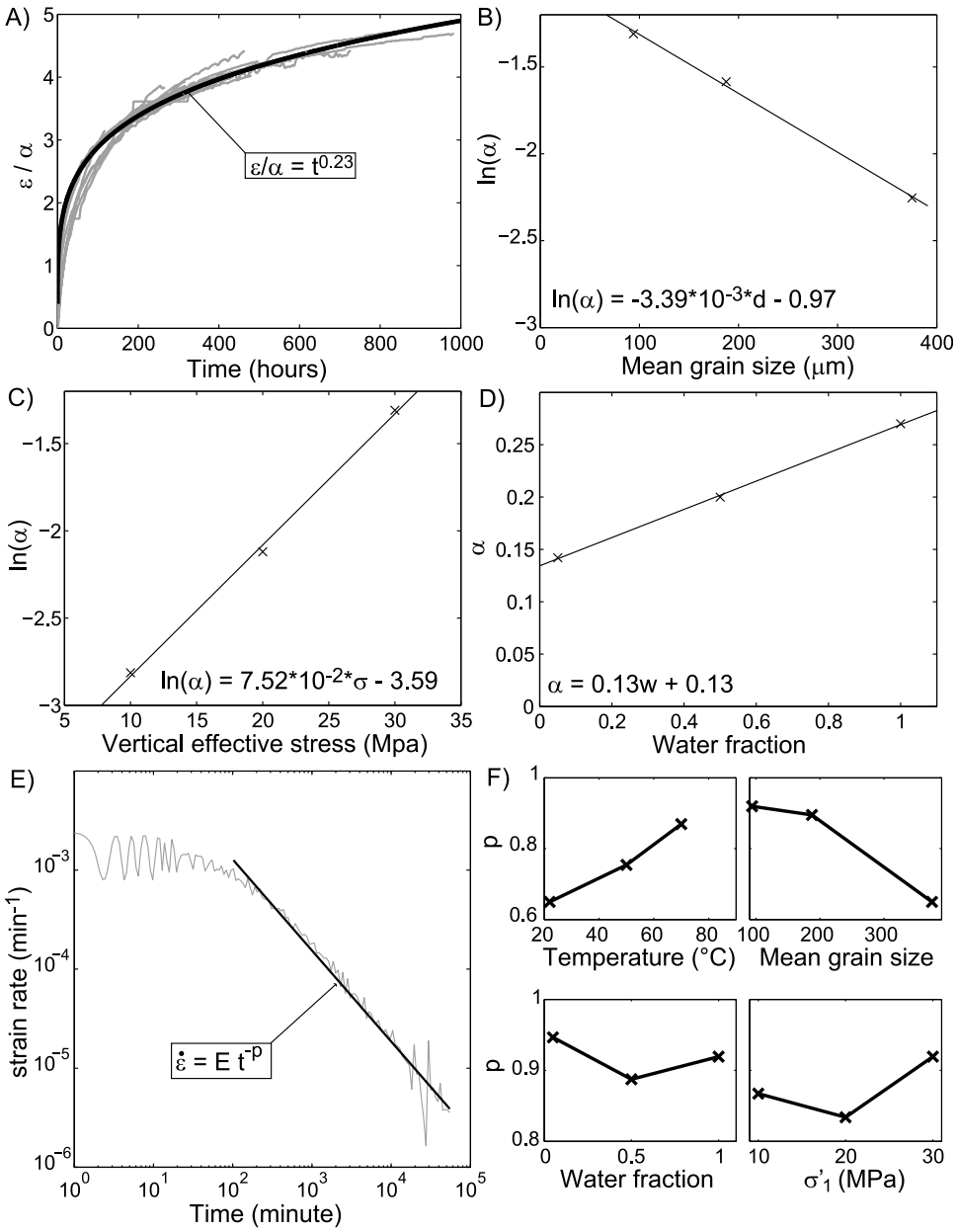


**Figure 8.** (a) Data collapsed onto a single curve and fitted by equation (5). (b) The parameter $\alpha$ as a function of effective uniaxial stress, (c) $\alpha$ as a function of mean grain size, and (d) $\alpha$ as a function of water fraction. (e) Strain rate versus time (log-log plot) for creep test T34. (f) The $p$ exponents as a function of parameters tested.

between compressibility of samples saturated with reactive and nonreactive fluids. More chemical compaction was observed in bioclastic samples than in crushed calcite samples. This is probably related to the fact that calcite is both thermodynamically more stable and less soluble than magnesian calcite [*Morse and Mackenzie*, 1990; *Stumm and Morgan*, 1996], and that the surface area available for chemical reaction was higher in the bioclastic carbonate sand. This suggests that at least part of the chemical compaction observed in bioclastic carbonate samples is related to carbonate dissolution. An other indication for active dissolution in the present study is that in samples saturated with reactive fluids the compressibility increased with decreasing grain size (Figures 3b and 3c). In finer grain-sized samples the mean coordination number is higher than in coarser samples [*Lange*, 1984], resulting in the observed increased dissolution in fine-grained samples saturated with a reactive fluid, i.e., pressure solution.

#### 4.1.2. Effect of Stress Corrosion

[44] Cracks propagated parallel to the main stress axis and the length of the cracks correlated positively with grain solubility and was therefore depending on the nature of the fluid (Figures 4c and 4d). Crack propagation occurred faster in water-saturated samples. In addition, compressibility of

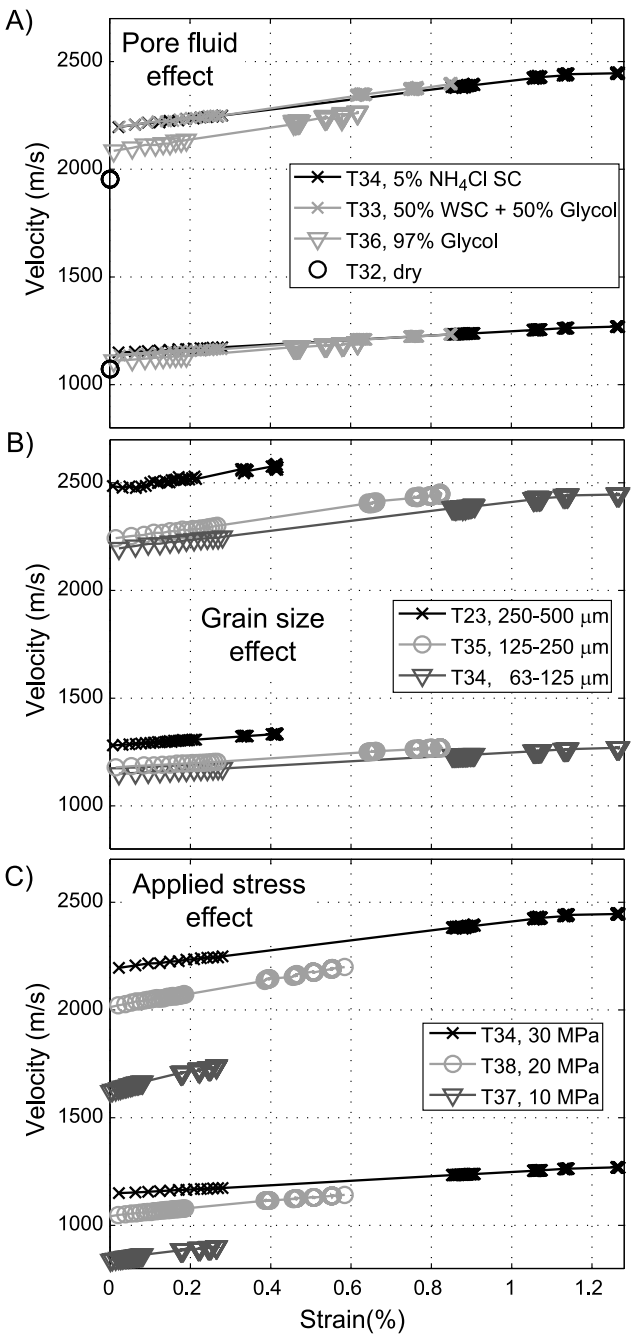


**Figure 9.** $V_p$ and $V_s$ as a function of strain at constant stress. Effect of the (a) pore fluid, (b) grain size, and (c) applied stress.

bioclastic sand was higher in the presence of glycol than decane (Table 3). Subcritical crack growth occurs in brittle material at stresses lower than the critical fracture stress and is sensitive to the fluid present [*Atkinson*, 1982]. The material resistance to crack, $G$, is a function of the surface energy, $\gamma$ such that $G = 2\gamma$. Therefore, lowering the surface energy facilitates crack propagation [*Olagnon et al.*, 2006]. The surface energy of carbonates is lowered by adsorption of water onto the mineral surface and creation of chemical bounds between Ca in carbonate and O in water [*Cygan et al.*, 2002]. Glycol contains two hydroxyls groups probably resulting in formation of a similar Ca-O bound as in water, which lower the surface energy. Formation of similar bounds is not possible between decane or air and calcite surfaces and explains why the cracks length was smaller in these fluids.

#### 4.1.3. Effects at the Grain Contacts

[45] For the bioclastic sand material, the internal grain porosity collapsed at the rim of the grain-to-grain contacts (Figure 4). This mechanism was active in all bioclastic carbonate sand experiments and independent of the pore fluid composition. The amount of grain crushing related to this mechanism seems, however, to be greater in samples saturated with reactive fluids (Figures 4a and 4b). Note that collapse of porous shell structures was described as a compaction mechanism in naturally occurring limestones [*Meyers*, 1980].

#### 4.1.4. Compaction Laws

[46] All the compaction curves were fitted by a stretched exponential law (equation (2)), also named the Kohlraush-Williams-Watts (KWW) law. Even though this law has been widely used to describe compaction in material science, it has traditionally not been used in rock physics. The KWW law fitted well the tests carried out on bioclastic carbonate samples saturated with nonreactive fluids (Figure 2c), i.e., the purely mechanical part of the compaction. This is in agreement with the fact that the KWW law is also used to describe relaxation in noncohesive granular media [*Richard et al.*, 2005]. Relaxation can be described as a set of processes driving the grains from an initial low-density state toward a more stable higher density packing [*Philippe and Bideau*, 2002]. During compaction of sand, relaxation occurs mainly by collective particle motion and grain sliding, i.e., grain rearrangement [*Ben-Naim et al.*, 1998; *Philippe and Bideau*, 2002], those are therefore most likely dominant mechanisms of deformation during mechanical compaction of the present bioclastic carbonate sand.

[47] The onset of grain crushing is assumed to start at the intersection between the two linear parts of the $\epsilon = f(\log(\sigma))$ curve (Figure 2a), that is around 2 to 3 MPa effective stress. Early initiation of grain crushing during compaction of carbonate sand was also observed by *Chuhan et al.* [2003]. Grain crushing was most likely the process explaining deviation of the present experimental compaction curves from the KWW law.

[48] An important result is that initial porosity is an important parameter controlling further compaction (Figures 2c, 2d, 2e, and 3b). The initial geometrical configuration of the grains determines the amplitude of the large-scale grain rearrangements [*Caglioti et al.*, 1997] and thus the amount of final relaxation. This result supports suggestion from earlier studies that initial porosity needs to be taken into account to predict subsequent compaction [*Royden and Keen*, 1980; *Sclater and Christie*, 1980].

[49] Since both calcite and bioclastic carbonate sand could be fitted by the same law, this suggests that compaction of other type of sediments could also be fitted by the KWW law. Also to be mentioned, the range of values for the $\beta$ parameter is rather narrow, 0.6–0.7, for bioclastic sand saturated with reactive fluids. To fit larger carbonate compaction data sets with the KWW law, a mean value of $\beta$ could be used. As a result, only one free parameter, $\tau$, would

**Table 5.** Water Analyses[a]

| Number | $Mg^{2+}$ | $Ca^{2+}$ | $Na^{+}$ | $K^{+}$ | Alk[b] |
|---|---|---|---|---|---|
| T7 before test | 60 | 161 | 35 | 3.3 | 14.40 |
| T7 after test | 244 | 243 | 250 | 15 | |
| T8 before test | 28 | 150 | 8 | 0.73 | 15.16 |
| T8 after test | 208 | 208 | 197 | 11.6 | |
| T35 before test | 81 | 213 | 280 | 12.7 | |
| T35 after test | 211 | 165 | 1300 | 63 | |
| T38 before test | 67 | 353 | 132 | 9 | |
| T38 after test | 261 | 540 | 790 | 57 | |

[a]Concentration are given in ppm.
[b]Alkalinity in meq $L^{-1}$.

be necessary to describe carbonate compaction using the KWW law.

### 4.2. Creep

#### 4.2.1. Chemical Effects

[50] The absence of observable creep in samples saturated with nonreactive fluids, while strain was observed in samples saturated with reactive fluids, indicate that creep was due to chemical reactions (Figure 7). The significant increase in both $Mg^{2+}$ and $Ca^{2+}$ concentrations in the fluid after tests also shows that dissolution of magnesian calcite occurred during experiments (Table 5). In addition the $Mg^{2+}$ concentration increased about 2 times more than the $Ca^{2+}$ concentration during the tests (Table 5). Taking into account the stoichiometric dissolution of the bioclastic carbonates, about 5 times more $Ca^{2+}$ than measured should be present in the pore fluid. This significant buildup of $Mg^{2+}$ relative to $Ca^{2+}$ indicates active calcite precipitation/cementation in the bioclastic system during creep.

#### 4.2.2. Chemical Compaction Rheology: Interplay Between Pressure Solution Creep and Stress Corrosion

[51] All the data could be fitted by a power law (equation (5)) with a single exponent (Figure 8a), in a similar way as done by *Renard et al.* [2001] for salt aggregates compacting by pressure solution. The time exponent $\theta = 0.23$ is different than the traditional exponent of 1/3 expected for Andrade creep. However, this Andrade exponent may depend on the active deformation process [*Vishnevskii et al.*, 1989]. Several studies in material science, where sample were deformed under compression in a creep regime showed similar power law, with an exponent varying between 0.18 and 0.5 [*Chari*, 1967; *Greener et al.*, 1980; *Vishnevskii et al.*, 1989].

[52] The time-independent compaction parameter ($\alpha_j$ in equation (5)) increased with decreasing grain size (Figure 8b). The increase of strain rate as a function of decreasing grain size is characteristic of various creep processes, among them pressure solution [*Weyl*, 1959]. The strong influence of the grain size on $\alpha$ is in agreement with pressure solution models in which the relaxation time constant is strongly dependent on the mean grain diameter [*Revil*, 1999; *Revil et al.*, 2006]. As opposed to pressure solution, the rate of aggregate compaction resulting from subcritical crack growth should be proportional to the grain size [*Cruden*, 1970; *Chantikul et al.*, 1990]. The compaction parameter, $\alpha$, was found to increase with both stress and water concentration (Figures 8c and 8d). Pressure solution and subcritical crack growth are sensitive to stress in a similar way [*Charles*, 1958; *Lehner*, 1990]. Both processes were most likely active in the present study since significant creep was observed not only in samples saturated with fluids where calcite is soluble, like water, but also in samples saturated with glycol or anisole in which calcite is hardly soluble. The comparison between the 50/50 mixed water/glycol T33 test and the 3/97 mixed water/glycol T36 test (Figure 7b) indicates that pressure solution is a more effective deformation process than subcritical crack growth in water based systems. While subcritical crack growth will dominate when samples are saturated with either anisole or glycol.

[53] In the present study final strain rates range from $2.82 \times 10^{-8}$ to $2.85 \times 10^{-6}$ $s^{-1}$. Earlier experimental studies of carbonate creep found strain rates comprised between $1.24 \times 10^{-9}$ and $3.49 \times 10^{-8}$ $s^{-1}$ when pressure solution is responsible for the compaction [*Zhang and Spiers*, 2005; *Zubtsov et al.*, 2005] and between $2.29 \times 10^{-8}$ and $1.86 \times 10^{-6}$ $s^{-1}$ when compaction is due to interactions between pressure solution and subcritical crack growth [*Liteanu and Spiers*, 2009; *Croizé et al.*, 2010b]. Based on these previous studies, the rates found in the present study indicate that both pressure solution and subcritical crack growth were active during creep.

#### 4.2.3. Comparison With Relaxation Processes in Fault Zones

[54] Strain rate decay as a function of time during primary creep can be described by different power laws, e.g., Omori's law for earthquakes [*Omori*, 1894] or Andrade's law for metals [*Andrade*, 1910] and many industrial materials [*Chari*, 1967; *Greener et al.*, 1980; *Vishnevskii et al.*, 1989]. The value of the time exponent $p$ is usually lower than one. In the present experiments, the strain rate decay can be expressed as a power law (equation (7) and Figure 8e), with $p$ ranging from 0.65 to 0.95, having a mean value of $p = 0.85$. This value is comparable to the one found in models of primary creep in brittle rocks [*Amitrano and Helmstetter*, 2006]. Similar variations of the $p$ exponent are also observed when fitting afterslip and aftershock data with the Omori law [*Schaff et al.*, 1998; *Helmstetter and Shaw*, 2009]. These studies showed that postseismic relaxation, i.e., fault afterslip, can be described with a $p$ exponent similar to the one describing relaxation of bioclastic carbonate sand or various granular material during creep in compression. However, it is difficult to conclude if the mechanisms are the same in such various and different systems.

### 4.3. Ultrasonic Velocities

[55] At low stresses, $V_p$ measurements lower than 1500 m $s^{-1}$ may be partly explained by a small undersaturation [*Knight et al.*, 1998], in the present case the skeletal grains internal porosity may not have been completely filled with water. However, this is not sufficient to explain the low velocity obtained. It is also difficult to understand the fact that velocities of samples saturated with reactive fluids are lower than velocity of dry samples. A possible explanation can be related to the dissolution at grain contacts of carbonates saturated with reactive fluids. At the same effective stress, samples saturated with reactive fluids were more compressible than samples saturated with nonreactive fluids. The link between compressibility and chemical processes made in section 3 must therefore be taken into account while interpreting the present ultrasonic velocity measurements. Crack propagation may also lower elastic wave velocity [*Couvreur et al.*, 2001], and reactive surface areas lower grain contact

stiffness [*Vanorio et al.*, 2010], which might also explain lower velocity measurements in samples saturated with reactive fluids (Figures 5a and 5b).

[56] The measured ultrasonic velocities were dependent on the actual effective stress values (Figures 5a and 5b). This known effect [*Hughes and Kelly*, 1953] is outlined by the fact that several samples of the present study having different porosities show similar velocities when subjected to the same effective stress (Figures 5a and 5b). This effect is even more clear when looking at the bulk modulus (Figure 5c). *P* wave velocities at specific stresses where plotted against porosity (Figure 5d) to better investigate the velocity-porosity relation. Fitting the experimental data to the existing PGSO rock physics model shows that the initial porosity should also be taken into account to predict the *P* wave velocity-porosity relation (Figure 5d).

[57] The velocity increase observed in coarser grained samples (Figure 6) can be explained by the presence of larger contact areas in coarser samples [*Sutton et al.*, 1957]. In samples saturated with reactive fluids, the positive correlation found between *P* wave acoustic impedance and grain size (Figure 6d) might be linked to the positive correlation between $\beta$ and grain size (Figure 3c). No such correlation was found in dry samples (Figures 6d and 3c).

[58] During creep tests the $V_p$ to $V_s$ ratio remained constant, in the range between 1.9 and 2.0. This is in agreement with other studies and allows differentiation between limestones and sandstones having lower velocity ratio [*Assefa et al.*, 2003]. Both during loading and creep phases velocity increased linearly with decreasing porosity, a feature in agreement with other studies of carbonate [*Nolen-Hoeksema et al.*, 1995; *Wang*, 1997].

### 4.4. Implications for Porosity Prediction in Sedimentary Basins

[59] In the present study, chemical compaction was active during the loading phase enabling the separation between mechanical and chemical compaction. Since chemical compaction is strongly time dependent, its amount depends upon the loading rate resulting in more chemical compaction with lower loading rate. This agrees with field observations where mechanical compaction patterns correlate positively with the sedimentation rate [*Scholle and Halley*, 1985].

[60] The compressibility of bioclastic carbonate sand was significantly higher when saturated with reactive fluids than when saturated with nonreactive fluids. This difference was not as marked for the crushed calcite samples. This illustrates that initial compaction of carbonates is highly dependent on the primary mineralogy. If the sediments are initially composed of unstable minerals, aragonite dissolution and precipitation of calcite will occur independently of stress [*Morse and Mackenzie*, 1990]. This is also true for magnesian calcite if $Mg^{2+}$ is removed or precipitated as dolomite. If such cementation occurs a mechanically stable framework may be produced preventing further mechanical compaction [*Kopaska-Merkel et al.*, 1994; *Croizé et al.*, 2010a]. However, in the case of thermodynamically stable low-magnesium calcite sediments like planktonic forams or coccolithophores, compaction will be driven by stress and the subsequent compaction can most likely be explained by processes described in this study.

[61] Magnesium is a known inhibitor of both calcite dissolution [*Arvidson et al.*, 2006] and calcite precipitation [*Berner*, 1975]. If the sediments are composed of magnesian calcite, as in this study, the potential buildup of $Mg^{2+}$ in the pore space might either reduce or prevent the porosity loss by slowing down the rate of pressure solution [*Zhang and Spiers*, 2005], precipitation of dolomite in the pore space might also occur. The inhibiting effect of $Mg^{2+}$ on pressure solution was also observed in shallow water carbonates of south Florida [*Schmoker and Halley*, 1982].

[62] The present experimental data show that only minor amounts of water is sufficient for chemical compaction to occur. This explains why field observations show that cementation can occur even if oil migrates through a reservoir [*McLimans and Videtich*, 1989]. Based on these observations oil emplacement in carbonate reservoirs may not stop compaction but rather result in a different compaction mechanism than in carbonate sediments saturated with water. This was observed in bioclastic carbonate samples saturated with glycol. Glycol was shown to have the same effect than oil on chalk compaction [*Risnes et al.*, 2003]. The results from the present study suggest that subcritical crack growth will be the main mechanism responsible for compaction in oil-filled carbonate sediments.

## 5. Conclusion

[63] Uniaxial compression tests were carried out on bioclastic carbonate sands and crushed calcite samples with grain size in the range 63–500 $\mu$m. In samples saturated with reactive fluids, e.g., glycol/water mixture or water in equilibrium with carbonate, significant chemical compaction was documented during the loading phase. Samples saturated with nonreactive fluids, e.g., air or decane, showed less strain at the same effective stress since the compaction was only mechanical. When saturated with reactive fluids, finer grained samples were more compressible than coarser grained samples due to chemical compaction. Chemical compaction occurred by pressure solution which was enhanced by the presence of cracks at the grain-to-grain contacts. Compaction related microstructures identified in thin sections support these findings.

[64] During creep tests carried out on bioclastic carbonate sand the deformation was mostly due to chemical reactions. Furthermore pore water analysis, and especially the evolution of the $Mg^{2+}/Ca^{2+}$ ratio, showed that magnesian calcite dissolved during experiments. In all the creep experiments, the strain versus time relation followed a power law in time, with a single exponent equal to 0.23. From this observation, it was inferred that the same deformation mechanisms were active in all the creep experiments. Overall it was found that a combination of pressure solution creep and subcritical crack growth (stress corrosion) was responsible for strain, and strain rates were in the range $2.88 \times 10^{-8}$ to $2.82 \times 10^{-6}$ $s^{-1}$.

[65] The compressibility of the samples was controlled by, in order of importance, grain size, stress, and water saturation. Pressure solution was most likely the dominant mechanism of compaction in samples saturated with water. Conversely, in samples saturated with glycol or anisole, subcritical crack growth was most likely the main mechanism of deformation.

[66] Ultrasonic velocity measurements showed that *P* and *S* waves velocities were in the range of 705–2440 and 535–1250 m $s^{-1}$, respectively. Low velocities were especially observed in samples saturated with reactive fluids. Dissolution and transport affecting the grain-to-grain contacts geometry and crack propagation are likely to be the reason for such velocity alteration.

[67] All these observations indicate that relaxation processes at work in a granular material can have universal behaviors in systems as different as sedimentary layers during burial or fault zones during the interseismic period. In all cases, the nature of the fluid, the initial grain packing, and the grain size represent important control parameters of the final strain and the strain rates for a given stress.

[68] **Acknowledgments.** The experiments were conducted at the Norwegian Geotechnical Institute (NGI). Gudmund Havstad is thanked for his help in the laboratory. Nils Martin Hanken is gratefully acknowledged for providing the bioclastic carbonate sand. Lars Grande, Paul Meakin, and Agnès Helmstetter are acknowledged for sharing helpful discussions and analysis.

## References

Amitrano, D., and A. Helmstetter (2006), Brittle creep, damage, and time to failure in rocks, *J. Geophys. Res.*, *111*, B11201, doi:10.1029/2005JB004252.

Anderson, O. L., and P. C. Grew (1977), Stress-corrosion theory of crack-propagation with applications to geophysics, *Rev. Geophys.*, *15*(1), 77–104, doi:10.1029/RG015i001p00077.

Andrade, E. N. da C. (1910), On the viscous flow in metals, and allied phenomena, *Proc. R. Soc. London, Ser. A*, *84*(567), 1–12, doi:10.1098/rspa.1910.0050.

Anselmetti, F. S., and G. P. Eberli (1993), Controls on sonic velocity in carbonates, *Pure Appl. Geophys.*, *141*(2–4), 287–323, doi:10.1007/BF00998333.

Arvidson, R. S., M. Collier, K. J. Davis, M. D. Vinson, J. E. Amonette, and A. Luettge (2006), Magnesium inhibition of calcite dissolution kinetics, *Geochim. Cosmochim. Acta*, *70*(3), 583–594, doi:10.1016/j.gca.2005.10.005.

Assefa, S., C. McCann, and J. Sothcott (2003), Velocities of compressional and shear waves in limestones, *Geophys. Prospect.*, *51*(1), 1–13, doi:10.1046/j.1365-2478.2003.00349.x.

Athy, L. F. (1930), Density, porosity, and compaction of sedimentary rocks, *AAPG Bull.*, *14*(1), 1–24.

Atkinson, B. K. (1982), Subcritical crack propagation in rocks: theory, experimental results and applications, *J. Struct. Geol.*, *4*(1), 41–56, doi:10.1016/0191-8141(82)90005-0.

Audet, D., and A. C. Fowler (1992), A mathematical model for compaction in sedimentary basins, *Geophys. J. Int.*, *110*(3), 577–590, doi:10.1111/j.1365-246X.1992.tb02093.x.

Bassinot, F., J. Marsters, L. Mayer, and R. Wilkens (1993), Variations of porosity in calcareous sediments from the Ontong-Java plateau, *Proc. Ocean Drill. Program, Sci. Results*, *130*, 653–661, doi:10.2973/odp.proc.sr.130.058.1993.

Ben-Naim, E., J. B. Knight, E. R. Nowak, H. M. Jaeger, and S. R. Nagel (1998), Slow relaxation in granular compaction, *Physica D*, *123*(1–4), 380–385, doi:10.1016/S0167-2789(98)00136-5.

Berner, R. (1975), The role of magnesium in the crystal growth of calcite and aragonite from sea water, *Geochim. Cosmochim. Acta*, *39*(4), 489–504, doi:10.1016/0016-7037(75)90102-7.

Berryman, J. G. (1995), Mixture theories for rock properties, in *Rock Physics and Phase Relations: A Handbook of Physical Constants*, edited by T. Ahrens, pp. 205–228, AGU, Washington, D. C.

Birch, F. (1960), The velocity of compressional waves in rocks to 10 kilobars, part 1, *J. Geophys. Res.*, *65*(4), 1083–1102, doi:10.1029/JZ065i004p01083.

Bjørlykke, K. (2003), Compaction (consolidation) of sediments, in *Encyclopedia of Sediments and Sedimentary Rocks*, edited by G. V. Middleton and M. J. Church, pp. 161–167, Kluwer Acad., Boston, Mass.

Caglioti, E., V. Loreto, H. J. Herrmann, and M. Nicodemi (1997), A "tetris-like" model for the compaction of dry granular media, *Phys. Rev. Lett.*, *79*(8), 1575, doi:10.1103/PhysRevLett.79.1575.

Chantikul, P., S. J. Bennison, and B. R. Lawn (1990), Role of grain size in the strength and r-curve properties of alumina, *J. Am. Ceram. Soc.*, *73*(8), 2419–2427, doi:10.1111/j.1151-2916.1990.tb07607.x.

Chari, S. S. (1967), Creep of carbon mixes at the temperature of extrusion, *Carbon*, *5*(1), 61–63, doi:10.1016/0008-6223(67)90107-8.

Charles, R. J. (1958), Dynamic fatigue of glass, *J. Appl. Phys.*, *29*(12), 1657–1662, doi:10.1063/1.1723019.

Christensen, N. I., and D. L. Szymanski (1991), Seismic properties and the origin of reflectivity from a classic Paleozoic sedimentary sequence, Valley and Ridge province, southern Appalachians, *Geol. Soc. Am. Bull.*, *103*(2), 277–289, doi:10.1130/0016-7606(1991)103<0277:SPATOO>2.3.CO;2.

Chuhan, F. A., A. Kjeldstad, K. Bjørlykke, and K. Høeg (2002), Porosity loss in sand by grain crushing; experimental evidence and relevance to reservoir quality, *Mar. Pet. Geol.*, *19*(1), 39–53, doi:10.1016/S0264-8172(01)00049-6.

Chuhan, F. A., A. Kjeldstad, K. Bjørlykke, and K. Høeg (2003), Experimental compression of loose sands; relevance to porosity reduction during burial in sedimentary basins, *Can. Geotech. J.*, *40*(5), 995–1011, doi:10.1139/t03-050.

Couvreur, J. F., A. Vervoort, M. S. King, E. Lousberg, and J. F. Thimus (2001), Successive cracking steps of a limestone highlighted by ultrasonic wave propagation, *Geophys. Prospect.*, *49*(1), 71–78, doi:10.1046/j.1365-2478.2001.00242.x.

Croizé, D., S. N. Ehrenberg, K. Bjørlykke, F. Renard, and J. Jahren (2010a), Petrophysical properties of bioclastic platform carbonates: Implications for porosity controls during burial, *Mar. Pet. Geol.*, *27*(8), 1765–1774, doi:10.1016/j.marpetgeo.2009.11.008.

Croizé, D., F. Renard, K. Bjørlykke, and D. K. Dysthe (2010b), Experimental calcite dissolution under stress: Evolution of grain contact microstructure during pressure solution creep, *J. Geophys. Res.*, *115*, B09207, doi:10.1029/2010JB000869.

Cruden, D. (1970), A theory of brittle creep in rock under uniaxial compression, *J. Geophys. Res.*, *75*(17), 3431–3442, doi:10.1029/JB075i017p03431.

Cygan, R. T., K. Wright, D. K. Fisler, J. D. Gale, and B. Slater (2002), Atomistic models of carbonate minerals: Bulk and surface structures, defects, and diffusion, *Mol. Simul.*, *28*(6–7), 475–495, doi:10.1080/08927020290030099.

Dürrast, H., and S. Siegesmund (1999), Correlation between rock fabrics and physical properties of carbonate reservoir rocks, *Int. J. Earth Sci.*, *88*(3), 392–408, doi:10.1007/s005310050274.

Eberli, G. P., G. T. Baechle, F. S. Anselmetti, and M. L. Incze (2003), Factors controlling elastic properties in carbonate sediments and rocks, *Leading Edge*, *22*(7), 654–660, doi:10.1190/1.1599691.

Ehrenberg, S. N. (2006), Porosity destruction in carbonates platforms, *J. Pet. Geol.*, *29*(1), 41–52, doi:10.1111/j.1747-5457.2006.00041.x.

Fabricius, I. L. (2003), How burial diagenesis of chalk sediments control sonic velocity and porosity, *AAPG Bull.*, *87*(11), 1755–1778, doi:10.1306/06230301113.

Fruth, L. S., G. R. Orme, and F. A. Donath (1966), Experimental compaction effects in carbonate sediments, *J. Sediment. Petrol.*, *36*(3), 747–754, doi:10.1306/74D7155F-2B21-11D7-8648000102C1865D.

Gassmann, F. (1951), Elasticity of high-porosity sandstone, *Vierteljahrsschr. Nat. Ges. Zurich*, *96*, 1–23.

Giles, M. R. (1997), *Diagenesis: A Quantitative Perspective—Implications for Basin Modelling and Rock Property Prediction*, Kluwer Acad., Dordrecht, Netherlands.

Goldhammer, R. K. (1997), Compaction and decompaction algorithms for sedimentary carbonates, *J. Sediment. Res.*, *67*(1), 26–35, doi:10.1306/D42684E1-2B26-11D7-8648000102C1865D.

Greener, E. H., K. Szurgot, and E. P. Lautenschlager (1980), Time-temperature behavior for creep of dental amalgam, *J. Biomed. Mater. Res.*, *14*(2), 161–171, doi:10.1002/jbm.820140207.

Hamilton, E. L. (1976), Variations of density and porosity with depth in deep-sea sediments, *J. Sediment. Petrol.*, *46*(2), 280–300, doi:10.1306/212F6F3C-2B24-11D7-8648000102C1865D.

Helmstetter, A., and B. E. Shaw (2009), Afterslip and aftershocks in the rate-and-state friction law, *J. Geophys. Res.*, *114*, B01308, doi:10.1029/2007JB005077.

Hughes, D. S., and J. L. Kelly (1953), Second-order elastic deformation of solids, *Phys. Rev.*, *92*(5), 1145, doi:10.1103/PhysRev.92.1145.

Karner, S. L., J. S. Chester, F. M. Chester, A. K. Kronenberg, and A. Hajash (2005), Laboratory deformation of granular quartz sand: Implications for the burial of clastic rocks, *AAPG Bull.*, *89*(5), 603–625, doi:10.1306/12200404010.

Knight, J. B., C. G. Fandrich, C. N. Lau, H. M. Jaeger, and S. R. Nagel (1995), Density relaxation in a vibrated granular material, *Phys. Rev. E*, *51*(5), 3957, doi:10.1103/PhysRevE.51.3957.

Knight, R., J. Dvorkin, and A. Nur (1998), Acoustic signatures of partial saturation, *Geophysics*, *63*(1), 132–138, doi:10.1190/1.1444305.

Kopaska-Merkel, D. C., S. D. Mann, and J. W. Schmoker (1994), Controls on reservoir development in a shelf carbonate: Upper Jurassic smackover formation of Alabama, *AAPG Bull.*, *78*(6), 938–959.

Lange, F. F. (1984), Sinterability of agglomerated powders, *J. Am. Ceram. Soc.*, *67*(2), 83–89, doi:10.1111/j.1151-2916.1984.tb09620.x.

Lehner, F. K. (1990), Thermodynamics of rock deformation by pressure solution, in *Deformation Processes in Minerals, Ceramics and Rocks*, edited by D. J. Barber and P. G. Meredith, pp. 296–333, Unwin Hyman, London.

Liteanu, E., and C. J. Spiers (2009), Influence of pore fluid salt content on compaction creep of calcite aggregates in the presence of supercritical $CO_2$, *Chem. Geol.*, *265*(1–2), 134–147, doi:10.1016/j.chemgeo.2008.12.010.

Mavko, G., T. Mukerji, and J. Dvorkin (2009), *The Rock Physics Handbook: Tools for Seismic Analysis of Porous Media*, 2nd ed., Cambridge Univ. Press, Cambridge, U. K., doi:10.1017/CBO9780511626753.

McLimans, R. K., and P. E. Videtich (1989), Diagenesis and burial history of great oolite limestone, southern England, *AAPG Bull.*, *73*(10), 1195–1205.

Meyers, W. J. (1980), Compaction in Mississippian skeletal limestones, southwestern New Mexico, *J. Sediment. Res.*, *50*(2), 457–474.

Morse, J. W., and F. T. Mackenzie (1990), *Geochemistry of Sedimentary Carbonates*, Elsevier, Amsterdam.

Nolen-Hoeksema, R. C., Z. Wang, J. M. Harris, and R. T. Langan (1995), High-resolution crosswell imaging of a west Texas carbonate reservoir: Part 5—Core analysis, *Geophysics*, *60*(3), 712–726, doi:10.1190/1.1443810.

Norris, A. N. (1985), A differential scheme for the effective moduli of composites, *Mech. Mater.*, *4*(1), 1–16, doi:10.1016/0167-6636(85)90002-X.

Olagnon, C., J. Chevalier, and V. Pauchard (2006), Global description of crack propagation in ceramics, *J. Eur. Ceram. Soc.*, *26*(15), 3051–3059, doi:10.1016/j.jeurceramsoc.2005.11.004.

Omori, F. (1894), On the aftershocks of earthquakes, *J. Coll. Sci. Imp. Univ. Tokyo*, *7*, 111–120.

Philippe, P., and D. Bideau (2002), Compaction dynamics of a granular medium under vertical tapping, *Europhys. Lett.*, *60*(5), 677, doi:10.1209/epl/i2002-00362-7.

Rafavich, F., C. H. S. C. Kendall, and T. P. Todd (1984), The relationship between acoustic properties and the petrographic character of carbonate rocks, *Geophysics*, *49*(10), 1622–1636, doi:10.1190/1.1441570.

Renard, F., D. Dysthe, J. Feder, K. Bjørlykke, and B. Jamtveit (2001), Enhanced pressure solution creep rates induced by clay particles; experimental evidence in salt aggregates, *Geophys. Res. Lett.*, *28*(7), 1295–1298, doi:10.1029/2000GL012394.

Revil, A. (1999), Pervasive pressure-solution transfer: A poro-visco-plastic model, *Geophys. Res. Lett.*, *26*(2), 255–258, doi:10.1029/1998GL900268.

Revil, A., P. Leroy, A. Ghorbani, N. Florsch, and A. R. Niemeijer (2006), Compaction of quartz sands by pressure solution using a cole-cole distribution of relaxation times, *J. Geophys. Res.*, *111*, B09205, doi:10.1029/2005JB004151.

Richard, P., M. Nicodemi, R. Delannay, P. Ribiere, and D. Bideau (2005), Slow relaxation and compaction of granular systems, *Nat. Mater.*, *4*(2), 121–128, doi:10.1038/nmat1300.

Risnes, R., H. Haghighi, R. I. Korsnes, and O. Natvik (2003), Chalk-fluid interactions with glycol and brines, *Tectonophysics*, *370*(1–4), 213–226, doi:10.1016/S0040-1951(03)00187-2.

Royden, L., and C. E. Keen (1980), Rifting process and thermal evolution of the continental margin of eastern Canada determined from subsidence curves, *Earth Planet. Sci. Lett.*, *51*(2), 343–361, doi:10.1016/0012-821X(80)90216-2.

Ruiz, F., and J. Dvorkin (2009), Sediment with porous grains: Rock-physics model and application to marine carbonate and opal, *Geophysics*, *74*(1), E1–E15, doi:10.1190/1.3033212.

Schaff, D. P., G. C. Beroza, and B. E. Shaw (1998), Postseismic response of repeating aftershocks, *Geophys. Res. Lett.*, *25*(24), 4549–4552, doi:10.1029/1998GL900192.

Schmoker, J. W., and R. B. Halley (1982), Carbonate porosity versus depth; a predictable relation for south florida, *AAPG Bull.*, *66*(12), 2561–2570.

Scholle, P. A., and R. B. Halley (1985), Burial diagenesis: Out of sight, out of mind! in Carbonate cements, in *Carbonate Cements*, edited by N. Schneidermann and M. H. Paul, *Spec. Publ. Soc. Econ. Paleontol. Mineral.*, *36*, 309–334.

Sclater, J. G., and P. A. F. Christie (1980), Continental stretching: An explanation of the post-mid-cretaceous subsidence of the central North Sea basin, *J. Geophys. Res.*, *85*(B7), 3711–3739, doi:10.1029/JB085iB07p03711.

Stumm, W., and J. J. Morgan (1996), *Aquatic Chemistry: Chemical Equilibria and Rates in Natural Waters*, 3rd ed., John Wiley, New York.

Sutton, G. H., H. Berckhemer, and J. E. Nafe (1957), Physical analysis of deep sea sediments, *Geophysics*, *22*(4), 779–812, doi:10.1190/1.1438417.

Vanorio, T., C. Scotellaro, and G. Mavko (2008), The effect of chemical and physical processes on the acoustic properties of carbonate rocks, *Leading Edge*, *27*(8), 1040–1048, doi:10.1190/1.2967558.

Vanorio, T., G. Mavko, S. Vialle, and K. Spratt (2010), The rock physics basis for 4D seismic monitoring of $CO_2$ fate: Are we there yet?, *Leading Edge*, *29*(2), 156–162, doi:10.1190/1.3304818.

Velleman, P., and D. Hoaglin (1981), *Applications, Basics, and Computing of Exploratory Data Analysis*, Duxbury, Pacific Grove, Calif.

Vishnevskii, I. I., L. D. Smirnova, and Y. N. Yarovoi (1989), Unsteady creep equation in refractory materials during monoaxial compression, *Refract. Ind. Ceram.*, *30*(1–2), 22–27, doi:10.1007/BF01292534.

Wang, Z. (1997), Seismic properties of carbonate rocks, in *Carbonate Seismology*, *Geophys. Dev. Ser.*, vol. 6, edited by I. Palaz and K. J. Marfurt, pp. 29–52, SEG, doi:10.1190/1.9781560802099.ch3.

Weller, J. M. (1959), Compaction of sediments, *AAPG Bull.*, *43*(2), 273–310.

Weyl, P. K. (1959), Pressure solution and the force of crystallization—A phenomenological theory, *J. Geophys. Res.*, *64*(11), 2001–2025, doi:10.1029/JZ064i011p02001.

Zhang, X., and C. J. Spiers (2005), Compaction of granular calcite by pressure solution at room temperature and effects of pore fluid chemistry, *Int. J. Rock Mech. Min. Sci.*, *42*, 950–960, doi:10.1016/j.ijrmms.2005.05.017.

Zubtsov, S., F. Renard, J. P. Gratier, D. K. Dysthe, and V. Traskine (2005), Single-contact pressure solution creep on calcite monocrystals, in *Deformation Mechanisms, Rheology and Tectonics: From Minerals to the Lithosphere*, edited by D. Gapais, J. P. Brun, and P. R. Cobbold, *Geol. Soc. Spec. Publ.*, *243*, 81–95, doi:10.1144/GSL.SP.2005.243.01.08.

K. Bjørlykke, D. Croizé, and J. Jahren, Department of Geosciences, University of Oslo, PO Box 1047, Blindern, 0316 Oslo, Norway. (delphine.croize@geo.uio.no)

F. Renard, LGCA, Université Joseph Fourier-Grenoble I, CNRS-Observatoire de Grenoble, BP 53, F-38041 Grenoble, France.